Cell Reports

Article

Hypoxia Triggers the Intravasation of Clustered Circulating Tumor Cells

Graphical Abstract

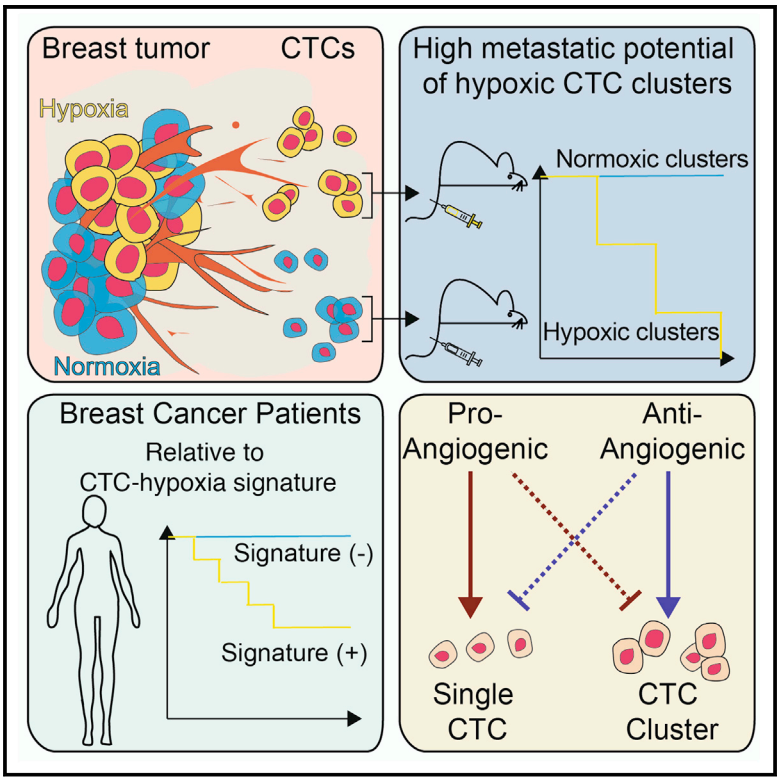

Authors

Cinzia Donato, Leo Kunz, Francesc Castro-Giner, ..., Andrea Banfi, Timm Schroeder, Nicola Aceto

Correspondence

nicola.aceto@unibas.ch

In Brief

Donato et al. show that intra-tumor hypoxia leads to cell-cell junction upregulation and formation of hypoxic CTC clusters with high metastatic ability. Treatment with EphrinB2 improves tumor vascularization and decreases hypoxia, leading to a reduced CTC cluster shedding rate and suppression of metastasis.

Highlights

- Hypoxia leads to cell-cell junction upregulation and intravasation of CTC clusters
- Hypoxic CTC clusters are highly metastatic compared to normoxic CTCs
- Increase in intra-tumor hypoxia leads to accelerated metastasis
- Treatment with EpB2 reduces hypoxia and prevents CTC cluster formation

Donato et al., 2020, Cell Reports *32*, 108105
September 8, 2020
https://doi.org/10.1016/j.celrep.2020.108105

CellPress

Cell Reports

CellPress
OPEN ACCESS

Article

Hypoxia Triggers the Intravasation of Clustered Circulating Tumor Cells

Cinzia Donato,[1] Leo Kunz,[2] Francesc Castro-Giner,[1,3] Aino Paasinen-Sohns,[1] Karin Strittmatter,[1] Barbara Maria Szczerba,[1] Ramona Scherrer,[1] Nunzia Di Maggio,[4] Wolf Heusermann,[5] Oliver Biehlmaier,[5] Christian Beisel,[2] Marcus Vetter,[6,7,8] Christoph Rochlitz,[7,8] Walter Paul Weber,[8,9] Andrea Banfi,[4] Timm Schroeder,[2] and Nicola Aceto[1,10,*]

[1]Department of Biomedicine, Cancer Metastasis Laboratory, University of Basel and University Hospital Basel, 4058 Basel, Switzerland
[2]Department of Biosystems Science and Engineering, ETH Zürich, 4058 Basel, Switzerland
[3]SIB Swiss Institute of Bioinformatics, 1015 Lausanne, Switzerland
[4]Department of Biomedicine, Cell and Gene Therapy Laboratory, University of Basel and University Hospital Basel, 4056 Basel, Switzerland
[5]IMCF Imaging Core Facility Biozentrum, University of Basel, 4056 Basel, Switzerland
[6]Gynecologic Cancer Center, University Hospital Basel, 4056 Basel, Switzerland
[7]Department of Medical Oncology, University Hospital Basel, 4056 Basel, Switzerland
[8]Breast Cancer Center, University Hospital Basel, 4056 Basel, Switzerland
[9]Department of Surgery, University of Basel and University Hospital Basel, 4056 Basel, Switzerland
[10]Lead Contact
*Correspondence: nicola.aceto@unibas.ch
https://doi.org/10.1016/j.celrep.2020.108105

SUMMARY

Circulating tumor cells (CTCs) are shed from solid cancers in the form of single or clustered cells, and the latter display an extraordinary ability to initiate metastasis. Yet, the biological phenomena that trigger the shedding of CTC clusters from a primary cancerous lesion are poorly understood. Here, when dynamically labeling breast cancer cells along cancer progression, we observe that the majority of CTC clusters are undergoing hypoxia, while single CTCs are largely normoxic. Strikingly, we find that vascular endothelial growth factor (VEGF) targeting leads to primary tumor shrinkage, but it increases intra-tumor hypoxia, resulting in a higher CTC cluster shedding rate and metastasis formation. Conversely, pro-angiogenic treatment increases primary tumor size, yet it dramatically suppresses the formation of CTC clusters and metastasis. Thus, intra-tumor hypoxia leads to the formation of clustered CTCs with high metastatic ability, and a pro-angiogenic therapy suppresses metastasis formation through prevention of CTC cluster generation.

INTRODUCTION

Circulating tumor cells (CTCs) are considered to be metastatic precursors in several cancer types, including breast cancer, but the mechanisms that lead to their generation from a solid tumor mass are poorly understood (Alix-Panabières and Pantel, 2014). CTCs are shed as single cells, as multicellular aggregates (CTC clusters), or in association with immune or stromal cells (Aceto et al., 2015; Duda et al., 2010; Gkountela et al., 2019; Szczerba et al., 2019). While cluster formation generally leads to an increased metastatic ability (Aceto et al., 2014, 2015; Cheung and Ewald, 2016; Cheung et al., 2016; Gkountela et al., 2019; Szczerba et al., 2019), whether CTC clusters are released from a cancerous lesion in a passive or active manner is unknown. Several factors have been linked to the ability of cancer cells to metastasize, such as cell-autonomous upregulation of metastasis-promoting genes (Bos et al., 2009; Kang et al., 2003; Massagué and Obenauf, 2016; Minn et al., 2005) or genes involved in the formation of a pre-metastatic niche (Esposito et al., 2018; Peinado et al., 2017), interaction with the immune system (Coffelt et al., 2015; Szczerba et al., 2019), or microenvironmental signals (Gilkes et al., 2014; Quail and Joyce, 2013).

Particularly in the context of the microenvironment, intra-tumor hypoxia and deregulated angiogenesis have emerged as key factors involved in cancer progression (Hanahan and Weinberg, 2011; Höckel and Vaupel, 2001; Jain, 2005). In contrast to healthy tissues, cancer cells are able to survive in hypoxic conditions and take advantage of the hypoxic microenvironment in multiple ways. For instance, hypoxia has been linked to chemotherapy and radiotherapy resistance of cancer cells (Comerford et al., 2002; Gray et al., 1953; Jain, 2005; Samanta et al., 2014) as well as increased metastasis formation (Rankin and Giaccia, 2016), and high levels of HIF1α expression—the master hypoxia regulator (Semenza, 1998)—correlate with a poor prognosis in patients with cancer (Baba et al., 2010). Anti-angiogenic therapies, typically targeting the vascular endothelial growth factor (VEGF) pathway (Vasudev and Reynolds, 2014), have been originally developed to reduce intra-tumor vasculature and consequently starve the tumor from its nutrients (Folkman, 1971). A growing body of evidence has also highlighted a vascular normalization signal for anti-angiogenic therapies as a function

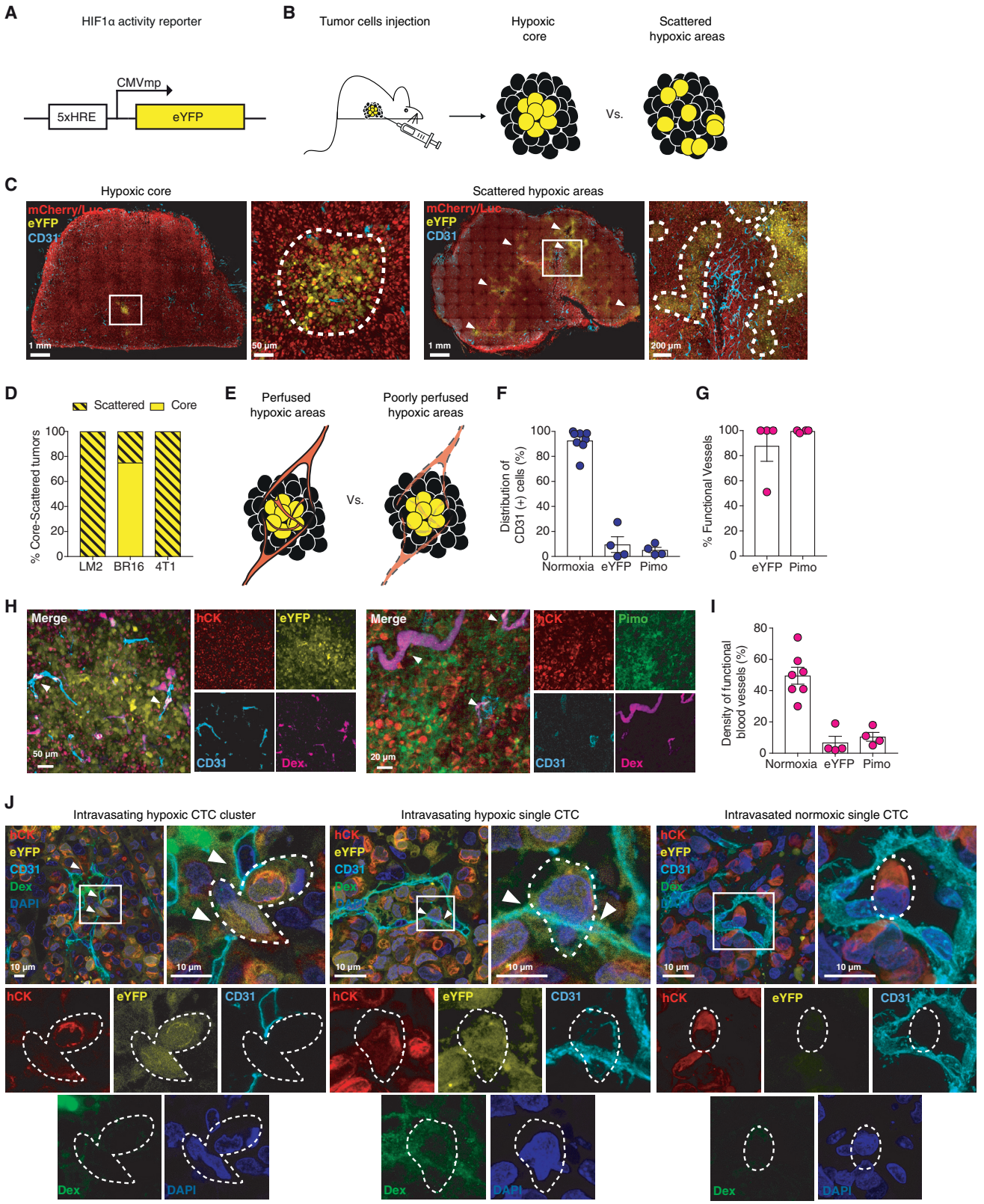

(legend on next page)

of tumor type as well as therapy dosage and schedule (Goel et al., 2011; Jain, 2013), unexpectedly resulting in improved blood flow, density, and mural cell coverage of blood vessels (Carmeliet and Jain, 2011). However, in breast cancer, anti-angiogenic treatments have failed to consistently prolong survival of patients, and paradoxically, intra-tumor hypoxia remains a hallmark of breast cancer biology (Gligorov et al., 2014; Jayson et al., 2016; Lang et al., 2013; Miller et al., 2007; Robert et al., 2011).

Several studies have suggested that hypoxic cancer cells are endowed with increased metastatic ability. Through HIF1α, hypoxia has been linked to metabolic changes during tumor progression, such as the transcription of genes encoding glucose transporters and glycolytic enzymes, favoring the Warburg effect (Mucaj et al., 2012; Semenza, 2010). Hypoxia has also been linked to phenotypic changes involved in cancer biology, such as an epithelial-to-mesenchymal transition (Lundgren et al., 2009). In a tumor, hypoxia is generally expected to be confined to the core and within regions that are poorly vascularized. However, this is an apparent paradox in the context of metastasis biology because metastatic cancer cells need to have access to functional blood vessels to achieve dissemination. We thought of tackling this controversy by directly addressing the role of hypoxia in spontaneous metastasis models *in vivo* and in relation to CTC generation and metastasis.

RESULTS

Hypoxic Areas Retain Functional Blood Vessels

We first sought to dynamically trace spontaneous hypoxic events by generating an activity reporter vector for HIF1α (HIF1α reporter) expressing enhanced yellow fluorescent protein (eYFP) under the control of hypoxia-response element (HRE) repeats (Figure 1A). We transduced the HIF1α reporter in human breast CTC-derived cells (BR16) directly obtained from a liquid biopsy (Gkountela et al., 2019), in human metastatic breast cancer cells (MDA-MB-231 lung metastatic variant, referred to as "LM2") (Minn et al., 2005), and in mouse breast cancer cells obtained from spontaneously arising primary tumors (4T1). We confirmed elevated eYFP levels both upon treatment with the HIF1α-stabilizer deferoxamine (DFO) (Figure S1A) and as a consequence to incubation in hypoxic conditions (0.1% O_2), compared to control cells and to cells exposed to 5% O_2 (Figures S1B and S1C). Of note, when transferring the cells back to normoxic (20% O_2) conditions, we could confirm the dynamic and reversible nature of our approach (Figures S1B and S1C). These results were also validated at the level of HIF1α protein expression (Figures S1D–S1F). As further controls, we confirmed that HIF1α knockdown completely abolished the ability of transduced cells to express eYFP and did not result in compensatory HIF2α expression (Figures S1G and S1H), and stimulation with reactive oxygen species (ROS) inducers or tricarboxylic acid cycle (TCA) metabolites failed to activate eYFP expression (Figure S1I), confirming the specificity of the reporter system.

We then injected reporter cancer cells into the mammary fat pad of immunocompromised (NOD scid gamma; NSG) mice and monitored spontaneous tumor development, aiming to visualize the emergence of hypoxic regions and determine their localization (i.e., either as hypoxic core or as scattered hypoxic areas) (Figure 1B). The expression of the HIF1α reporter did not alter tumor growth kinetics (Figure S2A), nor did it influence the overall course of the metastatic disease compared to control cells (Figure S2B). Primary tumors were then immunostained for mCherry (tumor cells), eYFP (HIF1α-expressing tumor cells), pimonidazole (gold standard to define hypoxic areas) (Varia et al., 1998), as well as CD31 (endothelial cells) to highlight intra-tumor hypoxic regions and the distribution of blood vessels throughout the tumor tissue. We observed a bimodal hypoxia distribution in tumors, either restricted within a central core or scattered throughout the tumor volume, yet in all cases characterized by distinct hypoxic regions with defined borders (Figures 1C, 1D, and S2C; Video S1). The percent of eYFP-positive or pimonidazole-positive cells within primary tumors varied between models and in individual mice, ranging from a mean of 5.6% to a mean of 64.1% (Figures S2D–S2F), with eYFP-positive cells co-localizing with pimonidazole regions in 31.1% to 54.9% of the cases (Figure S2G). As expected, the extent of the co-localization between eYFP and pimonidazole is influenced by the nature of the two methods: while eYFP is detectable only several hours after the establishment of hypoxia and labels cells that experienced prolonged hypoxic conditions to assemble eYFP (Figures S1A and S1B), pimonidazole uptake occurs rapidly in all areas that are

Figure 1. Dynamic Labeling and Assessment of Intra-Tumor Hypoxia

(A) Schematic representation of the HIF1α reporter.

(B) Schematic of the experimental design.

(C) Representative pictures of breast tumors displaying a hypoxic core (left) or scattered hypoxic areas (right).

(D) The plot shows the percentage of core versus scattered hypoxic areas in LM2, BR16, and 4T1 tumor models.

(E) Schematic of the experimental design.

(F) The plot shows the percentage of CD31-positive (+) cells within the normoxic and the hypoxic tumor areas of NSG-BR16-HIF1α reporter mice, defined HIF1α reporter (eYFP; n = 4), pimonidazole staining (Pimo; n = 4), or the lack of both (normoxia; n = 5).

(G) The plot shows the distribution in percentage of functional vessels within the hypoxic tumor areas of NSG-BR16-HIF1α reporter mice, defined by HIF1α reporter (eYFP; n = 4) or Pimo staining (n = 4).

(H) Representative images of NSG-BR16-HIF1α reporter tumors stained for human cytokeratin (hCK), eYFP, CD31, and Dextran (Dex) (left) or with hCK, Pimo, CD31, and Dex (right). White triangles highlight Dex-positive vessels.

(I) The plot shows the density in percentage of functional blood vessels in normoxic (n = 7), eYFP (n = 4), or Pimo-stained (n = 4) areas of NSG-BR16-HIF1α reporter tumors.

(J) Representative images of NSG-BR16-HIF1α reporter tumors stained for hCK, eYFP, CD31, and Dex and showing intravasating eYFP−(+) CTC cluster (left), intravasating eYFP−(+) single CTC (middle), and intravasated eYFP−(−) single CTC (right). White triangles highlight the intravasation sites.

For all panels, the error bars represent the SEM. See also Figures S1 and S2.

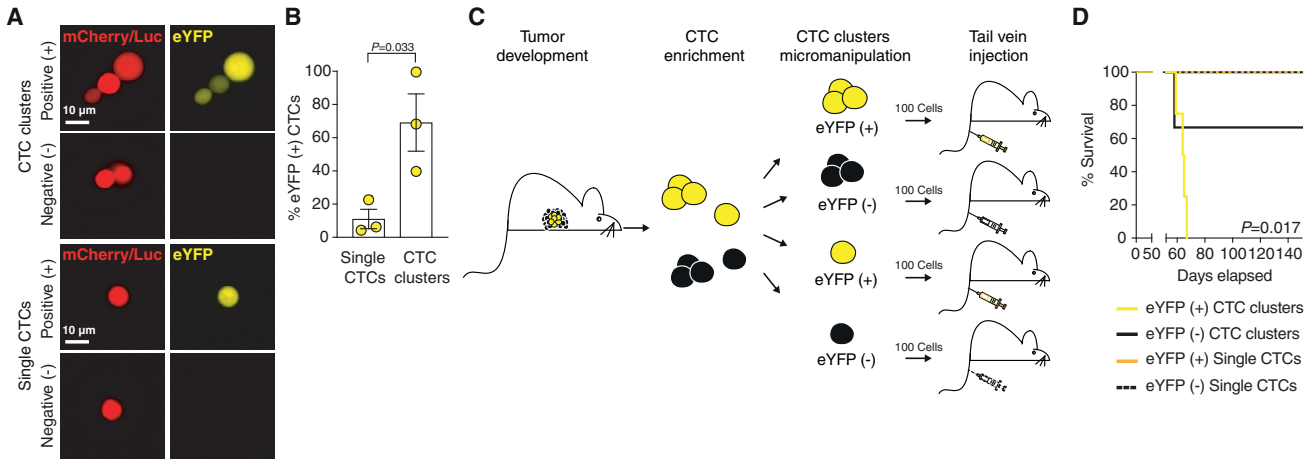

Figure 2. Dynamic Labeling of Hypoxic CTCs and Assessment of Their Metastatic Potential

(A) Representative pictures of CTC clusters (top) and single CTCs (bottom) from NSG-LM2-HIF1α reporter mice, positive (+) or negative (−) for eYFP expression.

(B) The plot shows the mean percentage of eYFP−(+) single CTCs (n = 3) and CTC clusters (n = 3) from NSG-LM2-HIF1α reporter mice. Error bars represent SEM; p value by two-tailed unpaired Student's t test is shown.

(C) Schematic of the experimental design.

(D) Kaplan-Meier survival analysis of NSG mice injected with eYFP−(+) (n = 4) or eYFP−(−) (n = 3) CTC clusters or single CTCs. p value by log-rank test is shown. See also Figures S3 and S4.

hypoxic at the moment of the exposure of tumor cells to the compound (Varia et al., 1998).

Next, we asked whether hypoxic regions of the tumor are perfused by functional blood vessels (Figure 1E). To this end, we intravenously injected dextran in tumor-bearing mice and assessed its presence within the vasculature of both hypoxic and normoxic regions. First, we found that CD31-positive cells (i.e., endothelial cells) are present throughout the tumor (Figure S2H) and distributed in both hypoxic and normoxic regions, with a higher presence in normoxic tumor regions (Figures 1F and S2I). Of note, the vast majority of blood vessels found in either eYFP- or pimonidazole-positive tumor areas also resulted positive for dextran, suggesting their functionality (Figures 1G, 1H, S2J, and S2K), while the density of functional blood vessels was higher in normoxic tumor regions compared to hypoxic ones, as expected (Figures 1I and S2L). Lastly, intravasation events were observed for eYFP-positive cancer cells in dextran-positive vessels (Figure 1J). Altogether, these results suggest that intra-tumor hypoxia occurs in spatially defined areas that are characterized by the presence of functional blood vessels, albeit at a lower density compared to normoxic tumor regions, highlighting a possible intravasation route for hypoxic cancer cells to the circulation.

CTC Clusters Originate from Hypoxic Tumor Regions

We next investigated the hypoxic status of live CTCs, spontaneously originating from tumor-bearing mice. To this end, we made use of the HIF1α reporter through eYFP detection, and not pimonidazole, for two main reasons. First, pimonidazole staining requires fixation, which would not allow us to perform functional assays with the isolated CTCs. Second, differently from pimonidazole, eYFP labels cells that experienced hypoxia for several hours, presumably starting at the level of the primary tumor given the short half-life of CTCs in circulation (Aceto et al., 2014), allowing us to focus on consolidated hypoxic events leading to sustained HIF1α activity. We first established that the number and composition of spontaneously generated CTCs were not altered by the expression of our HIF1α reporter system (Figure S3A). Strikingly however, we found that while the majority of single CTCs are normoxic (i.e., eYFP negative), CTC clusters are largely hypoxic in all three tested models (Figures 2A, 2B, S3B, and S3C), with the majority of the cells in each cluster being eYFP positive (Figures S3D–S3G). Of note, despite the fact that in the slow-growing BR16 model only a mean of 5.6% of primary tumor cells was eYFP positive (Figure S2E), we found a mean of 80.6% of CTC clusters to be positive for eYFP (Figure S3C), strongly suggesting their origin from hypoxic tumor areas and arguing against stochastic CTC intravasation dynamics.

To assess whether hypoxic CTC clusters are endowed with a greater metastatic potential compared to their normoxic counterparts, we first injected LM2-HIF1α reporter cells in the mammary fat pad of NSG mice, and upon tumor development, spontaneously generated single CTCs and CTC clusters were individually isolated, micromanipulated, and separated into "eYFP positive" or "eYFP negative" (Figure 2C). We found a higher ratio of Ki67-positive cells among hypoxic CTCs (both single and clustered) (Figures S3H–S3J). While hypoxic CTC clusters were generally found to contain a higher number of cells (a mean of 5.3 cells per hypoxic CTC cluster versus a mean of 2.82 cells per normoxic CTC cluster; $p < 0.001$) (Figure S3K), we intravenously injected a total of 100 cells per recipient tumor-free mouse for all groups for direct assessment of their metastatic potential, without disrupting the multicellular structure of CTC clusters (Figure 2C). Mice injected with hypoxic CTC clusters developed metastasis earlier and survived for a shorter time than those injected with normoxic CTC clusters, highlighting the higher metastasis-seeding ability of hypoxic CTC clusters (Figure 2D). Hypoxic single CTCs were not endowed

CellPress
OPEN ACCESS

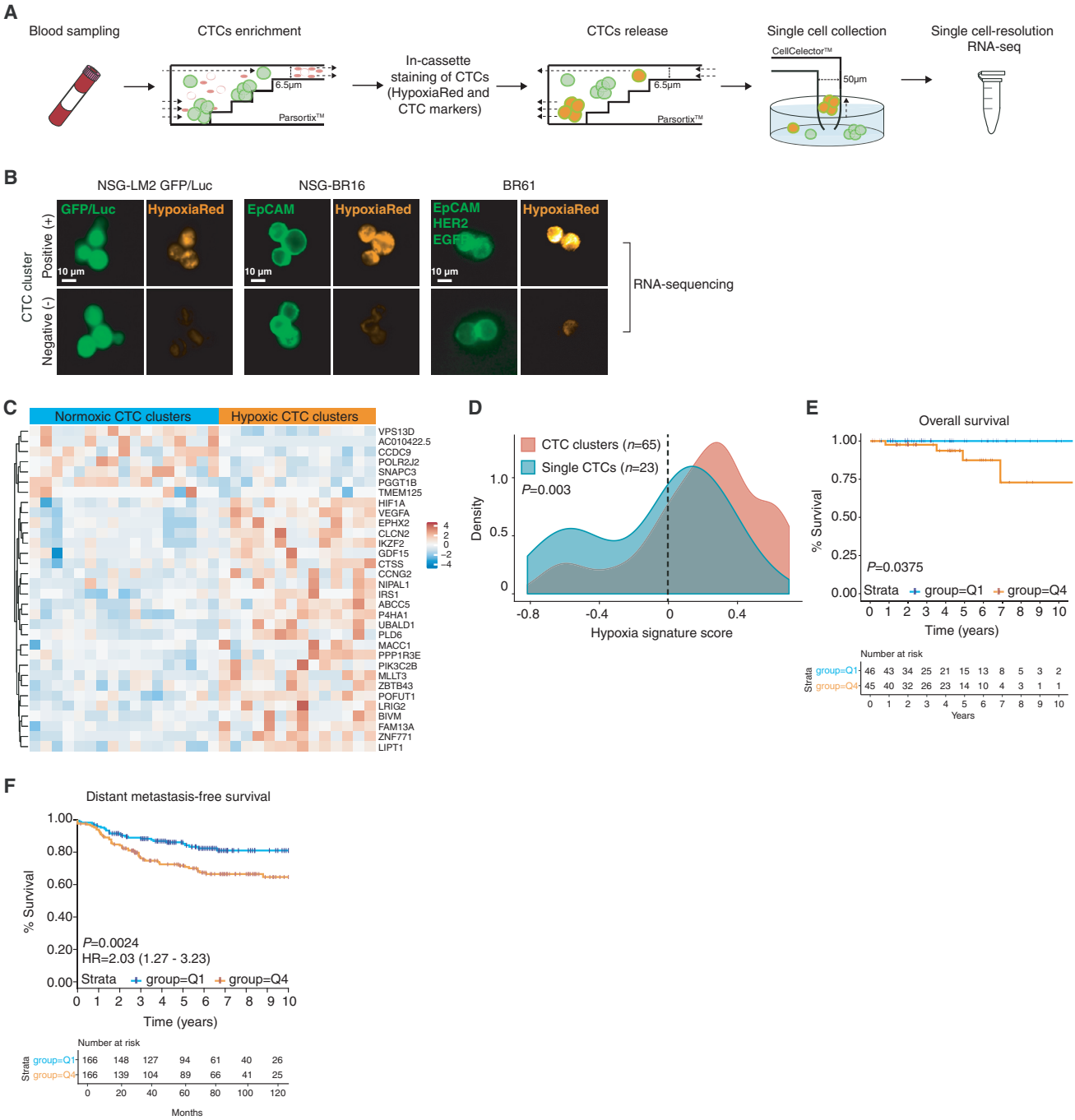

Figure 3. Hypoxic CTC Clusters Express a Gene Signature That Is Associated with a Poor Prognosis in Breast Cancer Patients

(A) Schematic of the experimental design.

(B) Representative pictures of CTC clusters from NSG-LM2-GFP/Luc, NSG-BR16 xenografts, and BR61 patient stained with HypoxiaRed and processed for RNA sequencing. The apparent cut in the HypoxiaRed-positive CTC cluster is due to the positioning of the CTC cluster relative to the pinhole.

(C) Heatmap showing differentially expressed genes between hypoxic (n = 14) and normoxic (n = 17) CTC clusters from NSG-LM2, NSG-BR16, and BR61 (FDR < 0.25).

(D) Density plot showing the distribution of CTC clusters and single CTCs from the GSE109761 dataset (n = 13 breast cancer patients) according to the expression of the hypoxic cluster signature. p value by one-tailed Student t test is shown.

(E) Overall survival rate of stage I breast cancer patients expressing in their primary tumor high (quantile 4, Q4) or low (quantile 1, Q1) levels of genes upregulated in hypoxic CTC clusters (top). The number of patients that progressed at each time point is shown (bottom). p value by log-rank test is shown.

(legend continued on next page)

with a greater metastatic ability compared to their normoxic counterparts, suggesting that hypoxia without clustering is not sufficient to increase the metastatic potential of cancer cells (Figure 2D). These findings are in line with previous publications highlighting the higher metastatic ability of CTC clusters compared to single CTCs (Aceto et al., 2014; Gkountela et al., 2019; Szczerba et al., 2019), given that the majority of clustered CTCs are found to be hypoxic. We also realized that virtually all CTC-white blood cell (WBC) clusters (Szczerba et al., 2019) from this model are hypoxic, and as expected, their direct metastatic ability exceeds that of hypoxic CTC clusters that were not associated with WBCs (Figures S3L–S3O). We then repeated the same experiment with the BR16-HIF1α model and confirmed the elevated metastatic ability of clustered hypoxic CTCs compared to their normoxic or single-cell counterparts (Figures S3P and S3Q).

Identification of a Hypoxic CTC Cluster Gene Signature

We next sought to interrogate the gene expression profile of hypoxic CTC clusters. To this end, we isolated live CTCs from a breast cancer patient (BR61) and two breast cancer xenografts (BR16 and LM2) and labeled them with HypoxiaRed, a cell-permeable dye that directly tags hypoxic cells based on their nitroreductase activity (Lizama-Manibusan et al., 2016), allowing gene expression profile comparison of hypoxic versus normoxic CTC clusters (Figure 3A). In contrast to eYFP, HypoxiaRed allowed us to label hypoxic CTCs independently of the exposure time to low oxygen concentrations, enabling the processing of live cells from freshly isolated blood samples. In control experiments, we demonstrate that HypoxiaRed positivity increases in hypoxic conditions (0.1% O_2) (Figure S4A), and it correlates with eYFP expression in HIF1α reporter cells and CTCs upon hypoxia induction (Figures S4B–S4E). In the same experiments, we also demonstrate that the vast majority of eYFP-positive CTCs (97%) from tumor-bearing mice stain positive for HypoxiaRed and pimonidazole, extending the validity of our approach (Figure S4E), and we detect a correlation between HypoxiaRed or eYFP intensity and CTC cluster size, as expected (Figure S4F). Lastly, to ensure that our procedure does not artificially create hypoxic cells, we intravenously injected normoxic LM2 cells in tumor-free mice, then processed blood samples at different time points (0, 15, and 30 min; consistent with the circulation half-life of CTC clusters) after injection and compared HypoxiaRed or eYFP positivity to control cells treated with DFO (Figure S4G). Importantly, we only found HypoxiaRed or eYFP positivity in control cells that were treated with DFO (Figure S4H), confirming that our procedure does not artificially create hypoxic cells.

Following CTC isolation and HypoxiaRed staining, in line with our previous findings, we observed a higher HypoxiaRed positivity in CTC clusters compared to in single CTCs (Figures S4I–S4K). We then individually micromanipulated a total of 28 HypoxiaRed-positive versus 33 HypoxiaRed-negative CTC clusters from xenografts and a patient sample and processed them for RNA sequencing (Figure 3B). Since hypoxic CTC clusters generally contain more cells than their normoxic counterparts (Figure S4L), typically resulting in a higher number of genes detected in single-cell RNA sequencing experiments (data not shown), we only considered 2- and 3-cell clusters for the RNA sequencing analysis in order to avoid technical biases. Differential expression analysis highlighted that hypoxic CTC clusters (as defined by HypoxiaRed positivity as well as expression of HIF1α and VEGFA; Figure S5A) differ in the expression of 32 genes (false discovery rate [FDR] < 0.25) compared to their normoxic counterparts (as defined by HypoxiaRed negativity and the absence of expression of HIF1α and VEGFA; Figure S5A), of which 25 upregulated and 7 downregulated (Figure 3C; Tables S1 and S2). In contrast, no changes were observed between hypoxic and normoxic clusters in terms of total number of detected genes or in the expression of genes related to cell cycle or epithelial-to-mesenchymal transition (Figures S5B–S5D). Among upregulated genes, in addition to HIF1α and VEGFA, we note GDF15, CCNG2, and P4HA1, previously associated with hypoxia (Fujimura et al., 2013; Lakhal et al., 2009; Xiong et al., 2018), as well as genes that were not previously linked to hypoxic conditions. To validate these findings, we evaluated the expression of our 25-gene signature found upregulated in hypoxic CTC clusters ("hypoxic cluster signature") in single and clustered CTCs (n = 88) from 13 breast cancer patients and found that our hypoxic cluster signature is significantly upregulated in CTC clusters (p = 0.003) (Figure 3D). We next tested whether our signature could predict the clinical outcome of breast cancer patients with early disease and no clinical evidence of metastasis (i.e., stage I, all subtypes from The Cancer Genome Atlas [TCGA] dataset) (Table S3). Strikingly, we found that low expression levels of the hypoxic cluster signature in the primary tumor correlate with 100% 10-yr survival rate of patients, while high expression levels predict a poor prognosis, as indicated by lower survival rates (p = 0.037) (Figure 3E). We observe that this predictive value is superior to previous hypoxia-related signatures (mostly obtained from *in vitro* data and bulk analyses) (Buffa et al., 2010; Elvidge et al., 2006; Ragnum et al., 2015; Winter et al., 2007) (Figure S5E). Lastly, in the advanced disease setting, we also find that high expression of the hypoxic cluster signature predicts a shorter metastasis-free survival (p = 0.0024) in a cohort of 1,746 breast cancer patients (Figure 3F).

Thus, hypoxia triggers the expression of a defined gene set in CTC clusters *in vivo*, highly predictive of a poor prognosis in breast cancer patients.

Proteomic Profiling of Hypoxic Cancer Cells

We next aimed at characterizing the protein expression profile of hypoxic and normoxic cancer cells directly isolated from the primary tumor of mice by means of an unbiased tandem mass tags-labeling strategy followed by mass spectrometry. We aimed to identify proteins that could mediate hypoxia-driven clustering *in vivo*. In particular, live primary tumor cells expressing the HIF1α reporter were digested and dissociated into single cells

(F) Distant metastasis-free survival rate of breast cancer patients expressing in their primary tumor high (Q4) or low (Q1) levels of genes upregulated in hypoxic CTC clusters (top). The number of patients that progressed at each time point is shown (bottom). p value by log-rank test is shown.
See also Figure S5 and Tables S1, S2, and S3.

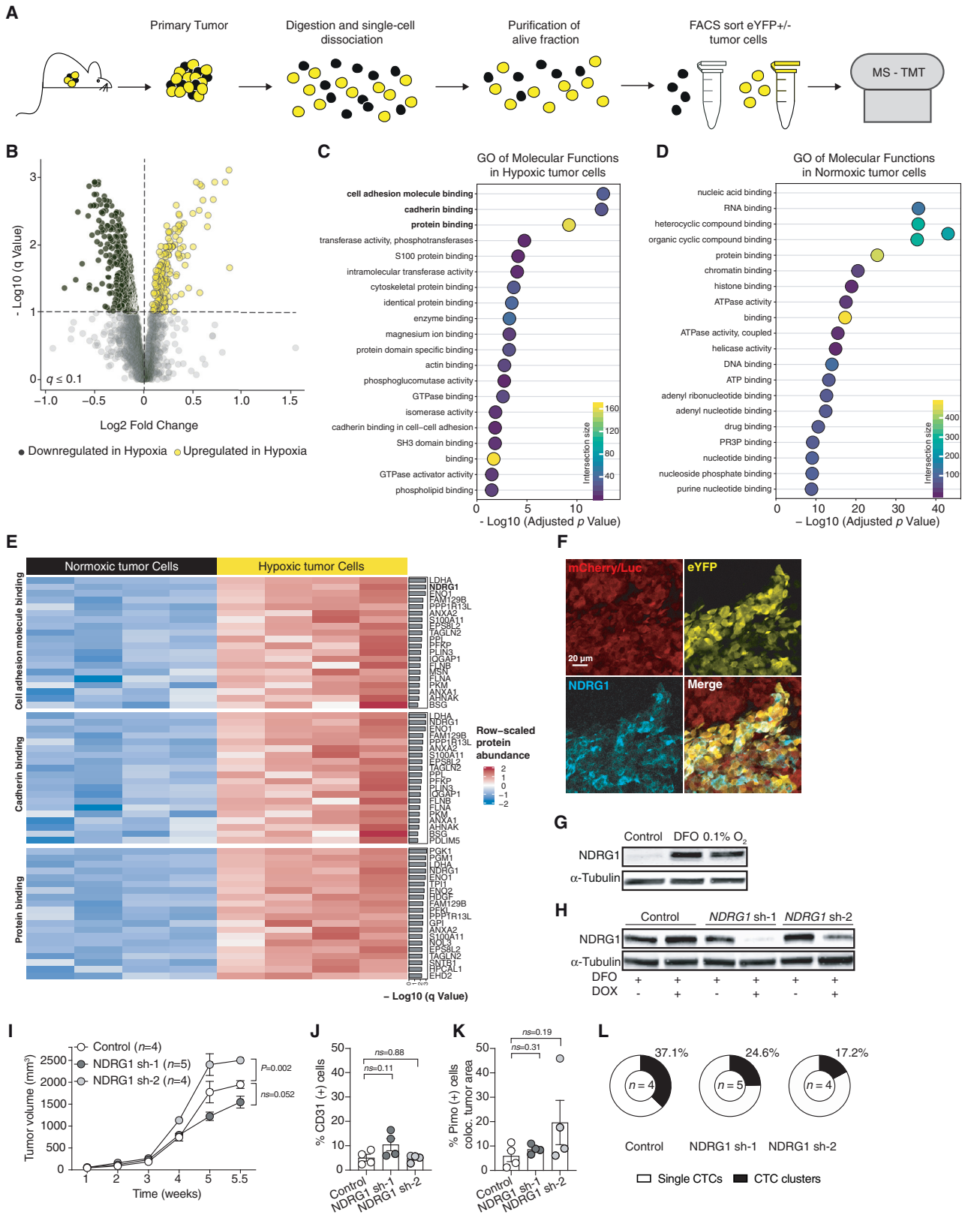

(legend on next page)

and sorted accordingly to eYFP expression prior to mass spectrometry analysis (Figure 4A). This strategy was chosen—as opposed to Hypoxia Red labeling—to allow protein production and assembly upon hypoxia induction, along with the expression of eYFP. Among 10,574 detected peptides, corresponding to 2,541 unique human proteins (Table S4), we found that 176 proteins are enriched in eYFP-positive tumor cells, while 498 are downregulated, compared to eYFP-negative tumor cells ($q \leq 0.1$; Figure 4B). Gene Ontology (GO) analysis of enriched proteins revealed upregulation of proteins involved in cell adhesion, cadherin, and protein binding (Figure 4C), consistent with a model whereby hypoxia leads to increased cancer cell clustering. In contrast, GO analysis of proteins upregulated in eYFP-negative tumor cells revealed enrichment in different molecular functions, including DNA and RNA binding (Figure 4D). Further, we isolated single and clustered CTCs, either positive or negative for eYFP, to investigate specific changes at the protein level occurring in circulation in addition to the primary tumor site (Figure S5F). Among 24,482 peptides (corresponding to 3,033 unique human proteins; Table S5) detected in hypoxic and normoxic CTCs, we found that 418 proteins are enriched in eYFP-positive CTCs (single and clustered) and 988 are downregulated, compared to eYFP-negative CTCs ($q \leq 0.1$; Figure S5G). GO analysis of the proteins upregulated in hypoxic CTCs revealed an enrichment in cell adhesion, cadherin, and protein binding (Figure S5H), strongly mirroring the pattern of hypoxic cells within the primary tumor, as expected, given the short half-life of CTCs in circulation (Aceto et al., 2014). Detailed analysis highlighted the involvement of several players including NDRG1, previously associated with hypoxia and cell-cell junction stability (Lachat et al., 2002) (Figure 4E). We further validated NDRG1 expression in pimonidazole-positive tumor areas of mice through immunohistochemistry staining (Figures 4F and S5I) and confirmed its elevated expression at the protein level upon hypoxia induction *in vitro* (Figure 4G). Next, we reasoned that given its upregulation as a consequence of hypoxia and its involvement in cell-cell junctions of epithelial cells, a lack of NDRG1 should not affect intra-tumor hypoxia levels, yet should negatively impact CTC cluster formation upon hypoxia induction. Consistently, we found that NDRG1 knockdown *in vivo* does not affect primary tumor size, abundance of CD31-positive cells, or intra-tumor hypoxia (Figures 4H–4K), but it decreases spontaneous CTC cluster generation (Figure 4L).

HIF1α Is Not Required for CTC Cluster Formation or Metastasis

We next tested whether HIF1α itself, beyond its role as an established hypoxia-associated transcription factor (Semenza, 1998), is also directly involved in the mechanisms that promote CTC cluster generation and their higher ability to metastasize. To this end, we generated inducible HIF1α knockdown in LM2 and BR16 cells, resulting in HIF1α suppression upon treatment with Doxycycline (Dox) (Figures 5A and 5B). We then injected these cells in the mammary fat pad of NSG mice and monitored primary tumor growth, CTC generation, and spontaneous metastasis formation upon Dox treatment. While Dox treatment successfully enabled the expression of HIF1α short hairpin RNAs (shRNAs) throughout the experiment *in vivo* (Figure 5C), we did not observe any differences in primary tumor size, CTC composition, metastasis formation, or overall survival between HIF1α knockdown and control mice (Figures 5D–5H). Pimonidazole staining also highlighted that HIF1α knockdown did not decrease the overall levels of intra-tumor hypoxia; rather, it increased them (Figure 5I). Given that VEGFA is a direct target of HIF1α transcriptional activity (Hicklin and Ellis, 2005), we then asked whether VEGFA expression was decreased as a consequence of HIF1α knockdown. Interestingly, we found that VEGFA mRNA levels were not altered upon HIF1α suppression (Figures 5J and 5K), confirming that in our cells, HIF1α is not the sole transcriptional activator of VEGFA (Pagès and Pouysségur, 2005). Along these lines, we also conclude that hypoxic cancer cells express high levels of HIF1α, VEGF, and NDRG1, among others, and while NDRG1 has been previously shown to be a target of several transcription factors including HIF1α (Said et al., 2017), its expression in hypoxic cells appears to be not exclusively controlled by HIF1α, given that HIF1α knockdown does not phenocopy the effects observed through NDRG1 depletion.

Figure 4. Hypoxic Tumor Cells Upregulate Cell-Cell Adhesion Proteins *In Vivo*

(A) Schematic of the experimental design.

(B) Volcano plot showing all the proteins detected with mass spectrometry analysis ($q \leq 0.1$).

(C) Gene ontology (GO) analysis of molecular function pathways upregulated in hypoxic tumor cells and ranked by adjusted p value.

(D) GO analysis of molecular function pathways upregulated in normoxic tumor cells and ranked by adjusted p value.

(E) Heatmap showing the expression levels of the top 20 upregulated proteins belonging to the GO terms enriched in hypoxic tumor cells. Ranking is based on q value.

(F) Representative pictures showing Pimo and human NDRG1 staining from LM2-HIF1α reporter tumor.

(G) Representative western blot shows NDRG1 protein in LM2-mCherry/Luc cells induced with either DFO or hypoxia (0.1% O_2).

(H) Representative western blot shows hNDRG1 protein in LM2-mCherry/Luc cells expressing a control shRNA (control), *NDRG1* shRNA-1, or *NDRG1* shRNA-2 (sh-1 and sh-2).

(I) The plot shows the mean tumor volume of NSG mice injected with LM2-mCherry/Luc expressing a control shRNA, *NDRG1* sh-1, or sh-2. p values by two-tailed unpaired Student's t test are shown.

(J) The plot shows the mean percentage of CD31−(+) cells within the primary tumor of LM2-mCherry/Luc mice expressing a control shRNA or *NDRG1* knockdown (n = 4). p values by two-tailed unpaired Student's t test are shown.

(K) The plots show the mean percentage of Pimo−(+) cells colocalizing with primary tumor cells of LM2-mCherry/Luc mice expressing a control shRNA or *NDRG1* knockdown (n = 4). p values by two-tailed unpaired Student's t test are shown.

(L) Pie charts displaying the mean percentage of single CTCs and CTC clusters in LM2-mCherry/Luc mice expressing a control shRNA or *NDRG1* knockdown.

For all panels, the number of independent biological replicates (n) is shown, and the error bars represent SEM. See also Figure S5 and Tables S4 and S5.

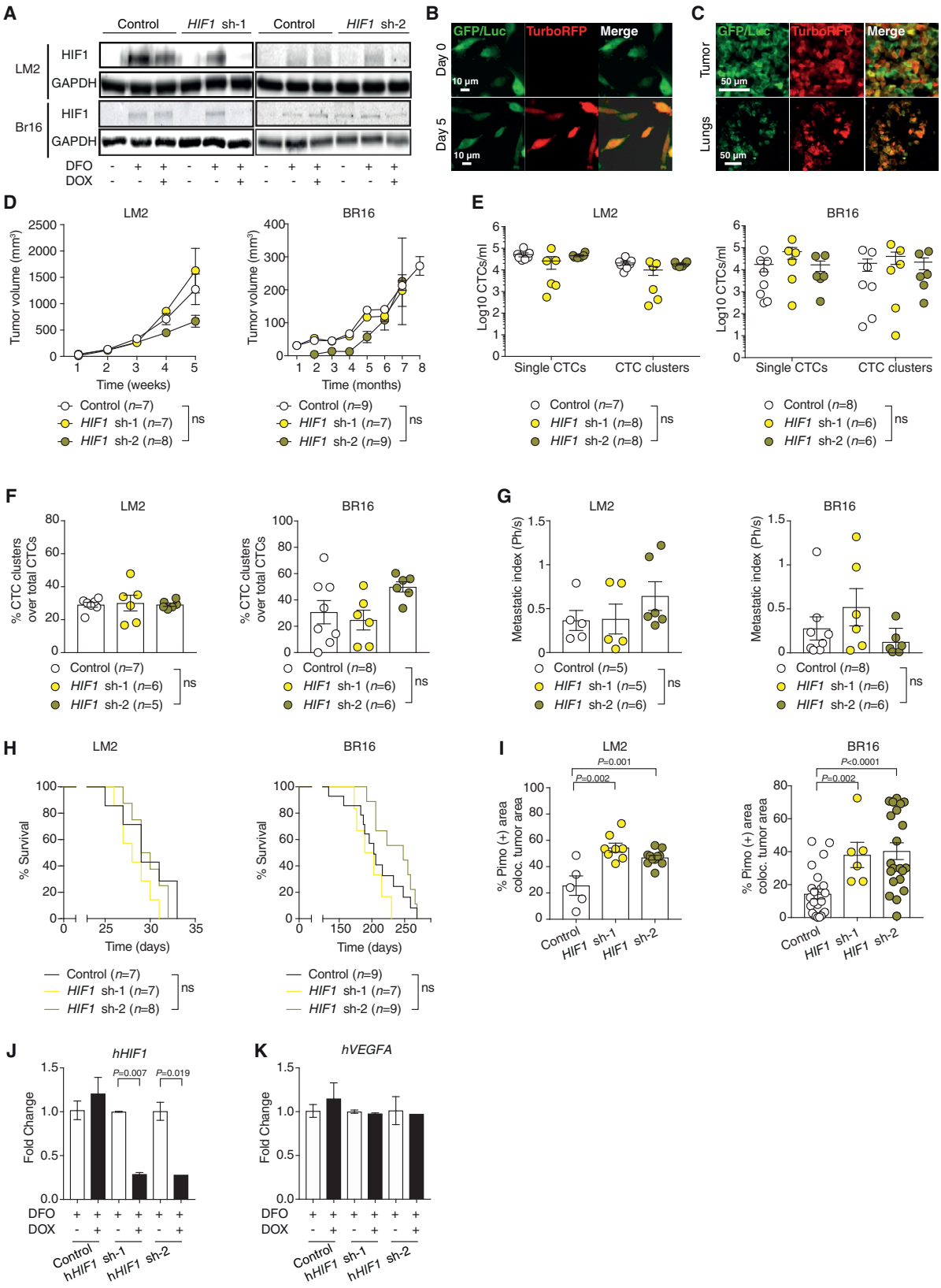

(legend on next page)

VEGFA Targeting Reduces Primary Tumor Size but Increases CTC Clusters and Metastasis

Given that VEGFA levels remain unaltered upon HIF1α suppression, we next asked whether the expression of VEGFA itself in cancer cells—as part of our hypoxic CTC clusters signature but also as a master angiogenesis regulator (Forsythe et al., 1996; Harper and Bates, 2008) and target of anti-angiogenic therapies (Vasudev and Reynolds, 2014)—could play a role in promoting CTC cluster generation and metastasis. To this end, we used Dox-inducible vectors expressing GFP along with shRNAs targeting the human or mouse VEGFA transcript and transduced them in LM2 or 4T1 cells, respectively. Upon Dox stimulation, we confirmed both the knockdown of VEGFA using two independent shRNAs as well as the expression of GFP (Figure S6A). We then injected LM2- and 4T1-shVEGFA cells in the mammary fat pad of NSG mice and monitored tumor progression. As expected, tumors expressing VEGFA shRNAs retained shRNA expression *in vivo*, grew slower and presented a decreased percent of CD31-positive cells relative to the total tumor area (i.e., fewer blood vessels), along with a higher positivity for pimonidazole (Figures 6A–6C and S6B–S6E). Strikingly, however, despite the slower growth rate of VEGFA knockdown tumors, we observed a remarkable increase in overall CTC counts and a shift toward CTC cluster production compared to control tumors of the same size (1,000 mm^3 for LM2 and 700 mm^3 for 4T1) in both models (from 11.4% to 24.5%–25.6% of CTC clusters in the LM2 model and from 25.8% to 32%–40.6% of CTC clusters in the 4T1 model) (Figures 6D–6F and S6F–S6H). The increased CTC cluster ratio and overall CTC counts also led to increased metastasis formation in animals bearing a VEGFA knockdown tumor (Figures 6G, 6H, S6I, and S6J). Of note, VEGFA knockdown did not influence the expression of HIF1α or HIF2α (Figure S6K). Given that VEGFA knockdown increases CTC cluster shedding and metastasis, we then asked whether treatment of mice with bevacizumab—an FDA-approved monoclonal antibody widely used for VEGFA targeting in cancer as well as other indications (Ferrara et al., 2004)—would phenocopy these results. We chose a high dose of bevacizumab to mimic our complete VEGFA suppression through shRNA expression, corresponding to 25 mg/kg (von Baumgarten et al., 2011). In full accordance with our VEGFA shRNA results, treatment with 25 mg/kg bevacizumab reduced primary tumor growth rate, accompanied by a decreased number of CD31-positive cells and increased pimonidazole positivity (Figures 6I–6K). Despite the smaller size of the primary tumor, bevacizumab-treated mice displayed a clear increase in overall CTC counts and CTC cluster production compared to larger control tumors (1,000 mm^3 for controls and 489 mm^3 for bevacizumab-treated mice), resulting in increased metastatic burden (Figures 6L–6P). Together, our results suggest that VEGFA targeting leads to tumor shrinkage, slower growth rate, and reduced vascularization, but it also promotes intra-tumor hypoxia, leading to increased CTC cluster shedding and accelerated metastasis formation.

A Pro-Angiogenic Therapy Suppresses Spontaneous Metastasis Formation

Based on our VEGFA targeting results, we then sought to address whether the opposite scenario (i.e., an increased tumor vascularization) could serve as a strategy to prevent the generation of CTC clusters and delay metastasis formation. We first tested our hypothesis in two fast-growing breast cancer models: LM2 and 4T1 injected in NSG mice. As a first step, we transduced both cell lines with a bicistronic construct expressing the mouse form of VEGFA ($_{m}VEGFA_{164}$) along with the truncated form of mouse CD8a transmembrane protein (mCD8aTr) (Ozawa et al., 2004), and then we selected clones with similar levels of $_{m}VEGFA_{164}$ expression, prospectively inferred through anti-mCD8aTr live staining (Figures S7A and S7B). We then injected two LM2- $_{m}VEGFA_{164}$-IRES-mCD8aTr clones (LM2-mVIC) and a control LM2-mCD8aTr clone (LM2-mC) in the mammary fat pad of NSG mice, simultaneously treated with either EphrinB2 Fc chimera protein—previously shown to activate EphB4 signaling and to ensure normal and functional angiogenesis along with elevated VEGFA levels (Groppa et al., 2018; Ozawa et al., 2004)—or Fc fragments as controls (Figure 7A). While

Figure 5. Knockdown of *HIF1α* Does Not Affect CTC Cluster or Metastasis Formation

(A) Representative western blot shows the human HIF1α protein in LM2-GFP/Luc (top) and BR16-GFP/Luc (bottom) cells expressing a control shRNA (control), h*HIF1α* shRNA-1, or h*HIF1α* shRNA-2 (sh-1 and sh-2).

(B) Representative pictures showing LM2-GFP/Luc cells upon knockdown.

(C) Representative pictures showing tumor (top) and metastatic lungs (bottom) of NSG-LM2-GFP/Luc mice expressing *HIF1α* shRNAs.

(D) The plots show the mean tumor volume of NSG mice injected with LM2-GFP/Luc (left) or BR16-GFP/Luc (right) and expressing a control shRNA or *HIF1α* knockdown. p values by two-tailed unpaired Student's t test are shown.

(E) Plots showing the log10 of total CTC counts per ml of blood obtained from NSG-LM2-GFP/Luc (left) or NSG-BR16-GFP/Luc (right) mice expressing a control shRNA or *HIF1α* knockdown. p values by two-way ANOVA are shown.

(F) The plots show the percentage of CTC clusters from NSG-LM2-GFP/Luc (left) or NSG-BR16-GFP/Luc (right) mice expressing a control shRNA or *HIF1α* knockdown. p values by two-tailed unpaired Student's t test are shown.

(G) The plot shows the metastatic index of NSG-LM2-GFP/Luc (left) or NSG-BR16-GFP/Luc (right) mice expressing a control shRNA or *HIF1α* knockdown. p values by two-tailed unpaired Student's t test are shown.

(H) Overall survival rates of NSG-LM2-GFP/Luc (left) or NSG-BR16-GFP/Luc (right) mice expressing a control shRNA or *HIF1α* knockdown. p value by two-sided log-rank test is shown.

(I) The plot shows the mean percentage of Pimo−(+) cells colocalizing with the primary tumor cells of NSG-LM2-GFP/Luc (left) or NSG-BR16-GFP/Luc (right) mice expressing a control shRNA control (n = 5 and n = 23) or *HIF1α* knockdown (sh-1, n = 8 and n = 6; sh-2, n = 11 and n = 21). p values by two-tailed unpaired Student's t test are shown.

(J) Plot showing *HIF1α* mRNA expression levels upon *HIF1α* knockdown (n = 2). p values by two-tailed unpaired Student's t test are shown.

(K) Plot showing h*VEGFA* mRNA expression levels upon *HIF1α* knockdown (n = 2).

For all panels, the number of independent biological replicates (n) is shown, and the error bars represent SEM.

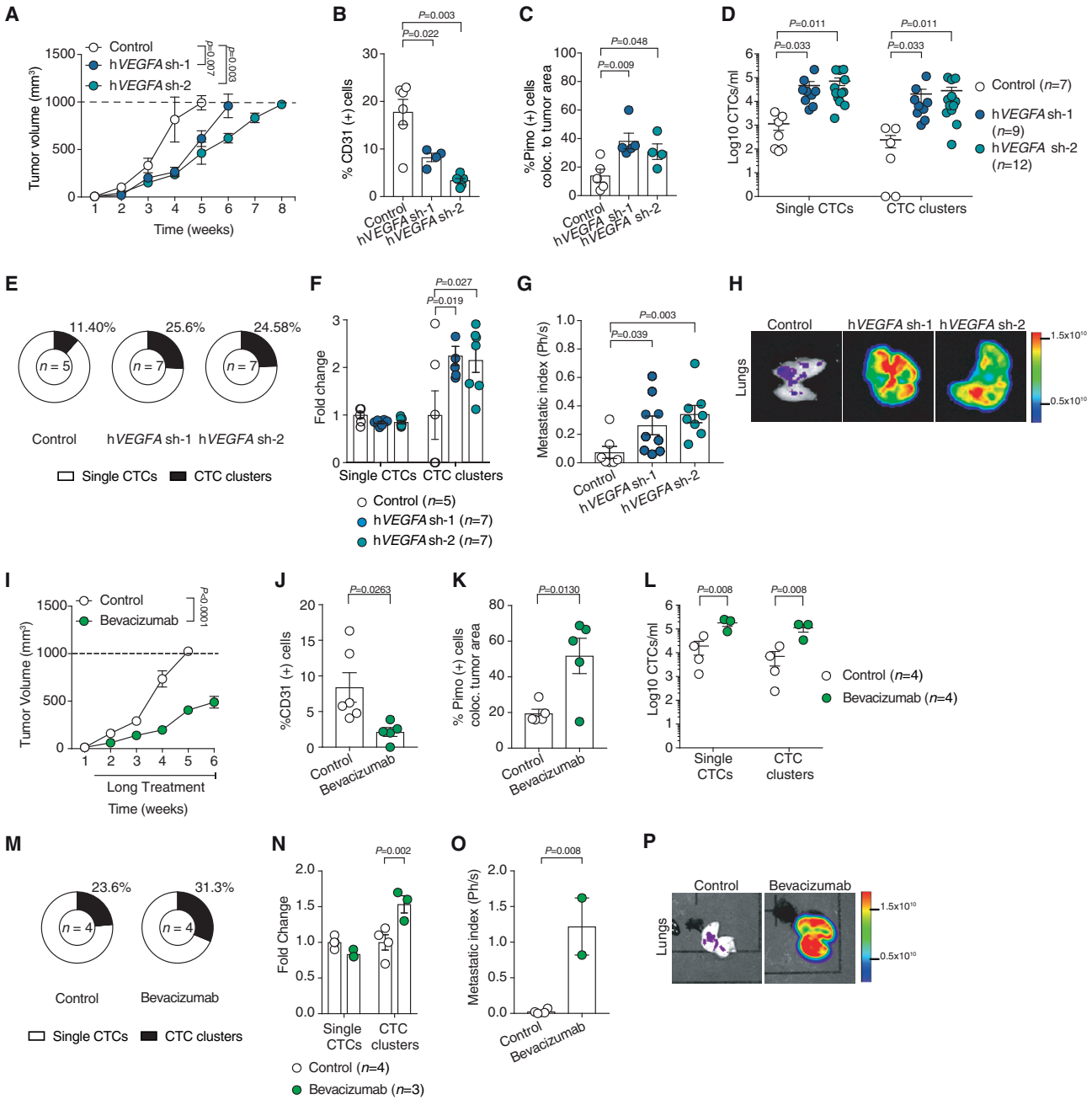

Figure 6. *VEGFA* Targeting Increases CTC Cluster Shedding and Metastasis Formation

(A) The plot shows the mean tumor volume of NSG mice injected with LM2-mCherry/Luc cells and expressing a control shRNA (control) or h*VEGFA* shRNAs (h*VEGFA* sh-1 and sh-2) (n = 7). p values by two-tailed paired Student's t test are shown.

(B) The plot shows the mean percentage of CD31-positive (+) cells within the primary tumor of NSG-LM2 mice expressing a control or *VEGFA* knockdown (n = 6 in control and sh-2; n = 4 in sh-1). p values by two-tailed unpaired Student's t test are shown.

(C) The plot shows the mean percentage of Pimo−(+) cells colocalizing with primary tumor cells of NSG-LM2 mice expressing a control or *VEGFA* knockdown (n = 3). p values by two-tailed unpaired Student's t test are shown.

(D) Plot showing the log10 of total CTC counts per ml of blood in NSG-LM2 mice expressing a control or *VEGFA* knockdown. p values by two-way ANOVA are shown.

(E) Pie charts displaying the mean percentage of single CTCs and CTC clusters in NSG-LM2 mice expressing a control or *VEGFA* knockdown.

(F) The plot shows the mean fold change of CTC ratios in NSG-LM2 mice expressing a control or *VEGFA* knockdown. p values by two-way ANOVA are shown.

(G) The plot shows the metastatic index of NSG-LM2 control (n = 7), NSG-LM2-h*VEGFA* sh-1 (n = 9), and sh-2 (n = 8) mice. p values by two-tailed unpaired Student's t test are shown.

(H) Representative bioluminescence images of lungs from NSG-LM2 mice expressing a control or *VEGFA* knockdown.

(legend continued on next page)

EphrinB2 or mVIC expression alone did not dramatically alter primary tumor growth rate, the simultaneous expression of mVIC and EphrinB2 treatment led to the formation of tumors characterized by a similar growth rate, yet able to reach the maximum allowed size in our license (2,800 mm^3) without causing any sign of distress in the tumor-bearing mice (Figure 7B). Primary tumor analysis revealed that LM2-mVIC tumors treated with EphrinB2 retained mVIC expression throughout the *in vivo* assay and also displayed increased CD31 positivity and decreased pimonidazole reactivity (Figures S7C–S7E), consistent with reduced intra-tumor hypoxia. Most importantly, despite having significantly larger tumors, mice with LM2-mVIC tumors treated with EphrinB2 generated fewer CTCs and displayed a reduced CTC cluster ratio compared to control animals (Figures 7C, 7D, and S7F), leading to a marked reduction in spontaneous metastasis formation and longer overall survival (Figures 7E, 7F, and S7G). As further confirmation in an independent model, we also observed a higher tumor growth rate associated with a longer overall survival in mice carrying a 4T1-mVIC tumor and treated with EphrinB2 (Figures S7H–S7K). Lastly, we asked whether these findings were reproducible in CTC-derived BR16 breast cancer cells, inherently characterized by the ability to form slow-growing tumors and displaying a higher number of functional vessels and lower intra-tumor hypoxia compared to the LM2 model (Figures 1G, S2F, and S2J). In this case, given the above, we tested whether the administration of EphrinB2 alone (i.e., without mVIC expression) would be sufficient to recapitulate the effects observed in the LM2 and 4T1 models. Treatment of BR16 xenografts with EphrinB2 led to the formation of significantly larger tumors (Figure 7G) characterized by higher CD31 positivity and reduced reactivity to pimonidazole (Figures S7L and S7M). Strikingly, EphrinB2-treated BR16 xenografts failed to generate CTC clusters (20.4% of CTC clusters for controls and 0% of CTC clusters for EphrinB2) and displayed overall reduced CTC shedding (Figures 7H, 7I, and S7N), leading to the suppression of spontaneous metastasis formation (Figures 7J and 7K). Of note, in all tested models, we find that Ephrin type-B receptor 4 (EphB4)—the target receptor of EphrinB2—is highly expressed in endothelial cells but not in cancer cells, arguing that EphrinB2 acts at the level of the endothelium (Figures S7O and S7P). Lastly, we tested whether a treatment with EphrinB2 could be beneficial in the advanced disease setting (i.e., when metastases are already established). We reasoned that even in a very late setting, a pro-angiogenic approach by means of EphrinB2 treatment could improve the tumor vasculature at metastatic sites and increase the delivery of tumor-killing drugs administered simultaneously (Stylianopoulos et al., 2018). To this end, we injected LM2 breast cancer cells through the tail vein of mice and waited for the development of growing lung metastases, *per se* sufficient to cause the death of the animal within a short period (i.e., without the need of further disease spread) (Figure 7L). Then, we administered either paclitaxel or EphrinB2 alone or a combination of the two agents and measured overall survival of treated mice. While EphrinB2 alone did not exert any beneficial effect (as expected, given that no new metastases were needed to be formed prior to experiment termination), a combination of EphrinB2 and paclitaxel outperformed all other conditions, including paclitaxel itself, confirming the beneficial effects of a pro-angiogenic therapy in combination with a tumor-killing agent in advanced disease settings (Figures 7L and 7M).

DISCUSSION

Our study suggests that intra-tumor hypoxia is a main trigger of the upregulation of cell-cell junction components and generation of hypoxic CTC clusters, endowed with a high proclivity to initiate metastasis. We propose that a pro-angiogenic therapy through treatment with EphrinB2 may increase vascularization and tumor growth rate, yet also suppress intra-tumor hypoxia and intravasation of clustered CTCs, leading to a reduction in metastasis formation.

A number of studies have linked intra-tumor hypoxia and HIF1α expression to metastasis formation (Rankin and Giaccia, 2016), but the actual impact of hypoxia in CTC biology is poorly understood. We find that hypoxic cancer cells present significantly upregulated cell-cell junction components, a property that promotes intravasation of clustered CTCs rather than individual ones and logically supports that hypoxic cancer cells in the bloodstream are most often found in the form of CTC clusters or CTC-WBC clusters. Surprisingly, we observe that hypoxic tumor areas are not devoid of functional blood vessels, highlighting possible accessibility routes for metastatic cells to the circulatory system. While this is important for explaining how hypoxic tumor cells can reach the periphery, whether intravasation events from hypoxic areas occur more frequently through veins (low intravascular oxygen levels) or arteries (high intravascular oxygen levels) remains to be defined. We use several methods to assess the hypoxic status of cancer cells during tumor progression, including direct staining with pimonidazole or

(I) The plot shows the mean tumor volume of NSG mice injected with LM2-mCherry/Luc cells and treated with isotype control (n = 4) or bevacizumab 25 mg/Kg (n = 5). p values by two-tailed unpaired Student's t test are shown.
(J) The plot shows the mean percentage of CD31−(+) cells within the primary tumor of NSG-LM2 mice treated with control or bevacizumab (n = 4). p values by two-tailed unpaired Student's t test are shown.
(K) The plot shows the mean percentage of Pimo−(+) cells colocalizing with primary tumor cells of NSG-LM2-mCherry/Luc mice treated with control or bevacizumab (n = 5). p values by two-tailed unpaired Student's t test are shown.
(L) Plot showing the log10 of total CTC counts per ml of blood in NSG-LM2-mCherry/Luc treated with control or bevacizumab. p values by two-way ANOVA are shown.
(M) Pie charts displaying the mean percentage of single CTCs and CTC clusters in NSG-LM2-mCherry/Luc treated with control or bevacizumab.
(N) The plot shows the mean fold change of CTC ratios in NSG-LM2 treated with control or bevacizumab. p values by two-way ANOVA are shown.
(O) The plot shows the metastatic index of NSG-LM2 treated with control (n = 4) or bevacizumab (n = 2). p values by two-tailed unpaired Student's t test are shown.
(P) Representative bioluminescence images of lungs from NSG-LM2 mice treated with control or bevacizumab.
For all panels, the number of independent biological replicates (n) is shown, and the error bars represent SEM. See also Figure S6.

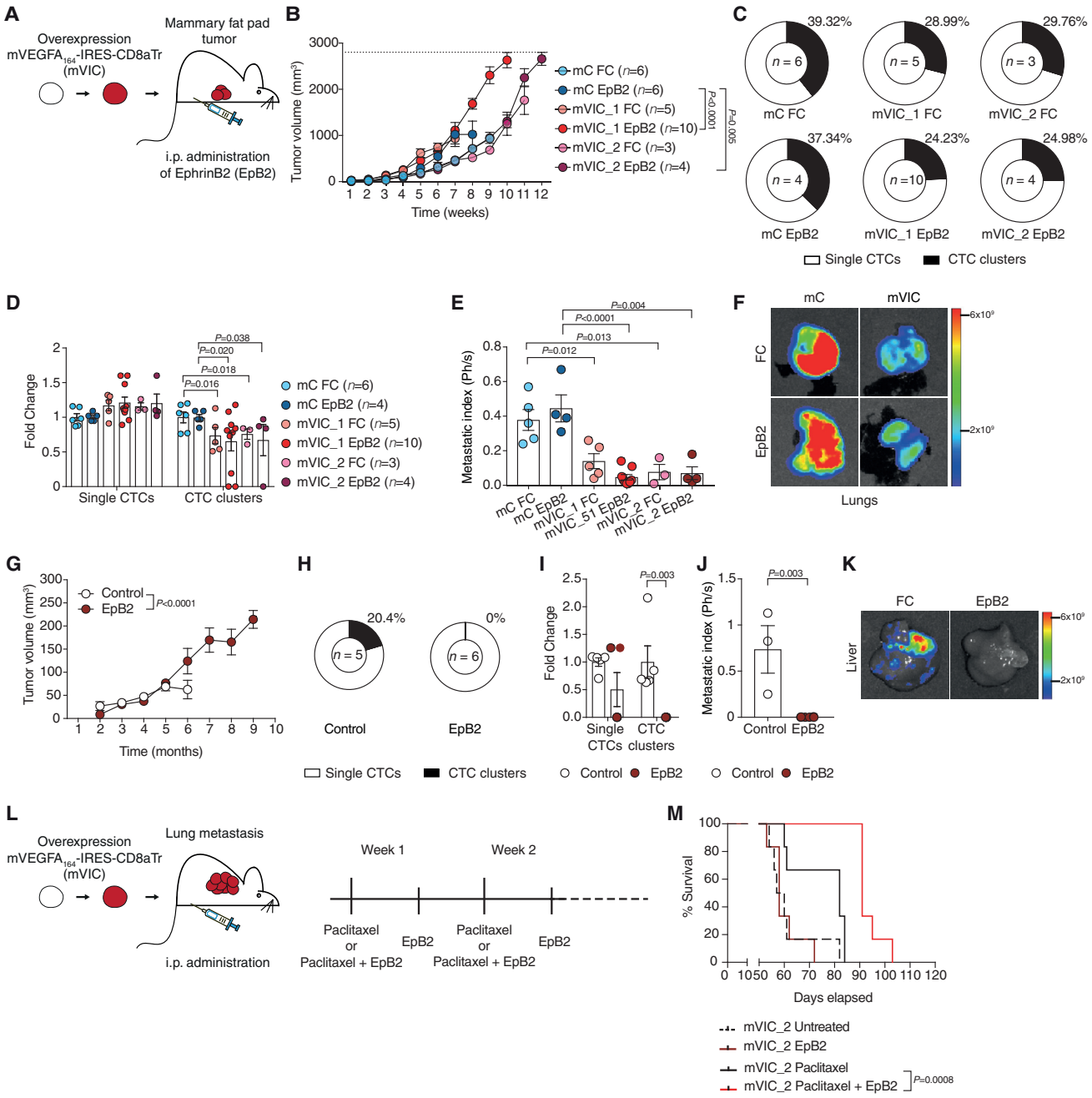

Figure 7. Pro-Angiogenic Therapy Reduces Intra-Tumor Hypoxia and Suppresses the Formation of CTC Clusters and Metastasis

(A) Schematic of the experimental design.

(B) The plot shows the mean tumor volume of NSG mice injected with LM2-mCherry/Luc cells expressing mVIC (mVIC) or control CD8aTr (mC), treated with either control FC fragments (FC) or EphrinB2 (EpB2). p values by two-tailed unpaired Student's t test are shown.

(C) Pie charts displaying the mean percentage of single CTCs and CTC clusters in NSG -LM2-mVIC or NSG-LM2-mC, treated with either FC or EpB2.

(D) The plot shows the mean fold change of CTC ratios in NSG-LM2-mVIC and NSG-LM2-mC, treated with FC or EpB2. p values by two-way ANOVA are shown.

(E) The plot shows the metastatic index of NSG-LM2-mVIC or NSG-LM2-mC mice, treated with FC or EpB2. p values by two-tailed unpaired Student's t test are shown.

(F) Representative bioluminescence images of metastatic lungs from NSG-LM2-mVIC or NSG-LM2-mC mice, treated with FC (top) or EpB2 (bottom).

(G) The plot shows the mean tumor volume of NSG-BR16-mCherry/Luc mice treated with FC (n = 5) or EpB2 (n = 5). p values by two-tailed unpaired Student's t test are shown.

(H) Pie charts displaying the mean percentage of single CTCs and CTC clusters in NSG-BR16-mCherry/Luc mice treated with FC or EpB2.

(legend continued on next page)

HypoxiaRed, in addition to a stably integrated eYFP-based reporter system. A combination of these is needed, given that each of these methods presents its own challenges, such as eYFP half-life leading to its persistence for a period of time upon hypoxia cessation, the need for fixation prior to pimonidazole staining limiting downstream molecular analysis, or the inability of HypoxiaRed to be used directly *in vivo*.

Hypoxic CTC clusters are destined to retain their hypoxic status at least until dissemination (i.e., the hypothesis that hypoxic CTC clusters may rapidly reacquire a normoxic status in circulation is highly unrealistic for several reasons). For instance, CTC clusters are characterized by a short circulation half-life (i.e., a few minutes; Aceto et al., 2014), most likely due to rapid physical entrapment in small capillary beds at distant sites. In this context, their biology is governed by events that occurred at the level of the primary tumor (e.g., the hypoxic microenvironment) and that are reflected during circulation. Based on our experiments aimed at assessing the metastatic potential of hypoxic and normoxic CTC clusters, features that characterize hypoxic CTC clusters appear to be key for metastasis seeding independently of the oxygen levels encountered in circulation or at the target metastatic site, and both hypoxic and normoxic cancer cells retain their original (hypoxic or normoxic) status while circulating. Further, the circulatory system alternates venous and arterial blood, where oxygen levels vary dramatically (Harrop, 1919). While CTCs are destined to collect in venous blood soon after they exit the tumor, whether they also experience arterial circulation mainly depends on the location of the extravasation site (e.g., upstream or downstream of the pulmonary circuit). Thus, both circulation half-life and the extravasation site are key parameters that influence a CTC's oxygen accessibility, and current data support a model whereby hypoxia (or normoxia) in CTCs reflects the condition that cancer cells experienced at the level of the primary tumor, just before intravasation.

VEGFA targeting is widely used in the clinical setting not only for cancer treatment, but also in other indications (Ferrara et al., 2007). Our experiments demonstrate that VEGFA suppression by means of shRNA expression or treatment with a high dose of bevacizumab results in tumor shrinkage—as previously shown in several models (Chiron et al., 2014; Gerber et al., 2000; Li et al., 2014)—but at the expense of reducing vascularization, leading to increased hypoxia. While these results are useful to gain important insights into the consequences of intra-tumor hypoxia for the metastatic process in breast cancer, it is important to underline that a large body of literature has also highlighted a vascular normalization effect for anti-VEGFA therapies as a function of therapy dosage and schedule (Jain, 2005, 2013), possibly influenced by tumor-intrinsic characteristics such as the extent and frequency of hypervascularized areas.

In our study, we make use of treatment with EphrinB2 (alone or in combination with VEGFA expression, depending on the growth rate of individual models) to achieve increased and normalized vascularization. EphrinB2 acts by binding and activating its receptor on endothelial cells, EphB4, achieving a regulation of intussusceptive angiogenesis and fine-tuning of endothelial proliferation induced by VEGF signaling (Groppa et al., 2018) and resulting into normal vessel formation and a reduction of intra-tumor hypoxia. Several other strategies may directly or indirectly lead to vascular normalization (Goel et al., 2011). These might be particularly interesting in the context of metastasis prevention, rather than for the effects that they exert on tumor growth. While this notion might be useful for the treatment of tumors that have not yet disseminated, we show that treatment of post-dissemination breast cancer (i.e., corresponding to stage IV disease) requires the co-administration of EphrinB2 with a tumor-killing agent, such as chemotherapy. In this context, Ephrin may not only prevent further metastasis-to-metastasis cascading disseminations, but also improve perfusion of the existing cancerous lesions, thus facilitating the tumor-killing activity of the co-administered compound. Clinical studies on well-defined patient populations will be key to address this point in the future.

Altogether, our study provides key insights into the role of hypoxia in CTC cluster generation. The next challenge will be to translate these findings to the clinical setting, as the optimal strategy might differ for individual patients as a function of their tumor subtype, organ location, and molecular characteristics, as well as the presence or absence of already-disseminated tumor cells with the ability to survive at distant sites. We speculate that therapies aimed at reducing intra-tumor hypoxia, alone or in combination with anticancer agents, may provide a new opportunity to blunt the metastatic spread of cancer in breast cancer patients.

STAR★METHODS

Detailed methods are provided in the online version of this paper and include the following:

- KEY RESOURCES TABLE
- RESOURCE AVAILABILITY
  - Lead contact
  - Materials availability
  - Data and code availability
  - Data and materials availability
- EXPERIMENTAL MODEL AND SUBJECT DETAILS
  - Human blood samples collection
  - Mouse blood samples collection
  - Cell lines

(I) The plot shows mean fold change of CTC ratios in NSG-BR16-mCherry/Luc treated with FC (n = 5) or EpB2 (n = 5). p values by two-tailed unpaired Student's t test are shown.
(J) The plot shows the metastatic index of NSG-BR16-mCherry/Luc mice treated with FC (n = 3) or EpB2 (n = 6). p values by two-tailed unpaired Student's t test are shown.
(K) Representative bioluminescence images of metastatic lungs from NSG-BR16-mCherry/Luc treated with FC (left) or EpB2 (right).
(L) Schematic of the experimental design.
(M) Overall survival rates of NSG-LM2-mVIC mice treated with paclitaxel, EpB2, or both. p value by two-sided log-rank test is shown.
For all panels, the number of independent biological replicates (n) is shown, and the error bars represent SEM. See also Figure S7.

SUPPLEMENTAL INFORMATION

Supplemental Information can be found online at https://doi.org/10.1016/j.celrep.2020.108105.

ACKNOWLEDGMENTS

We thank all patients who donated blood for our study, as well as all involved clinicians and study nurses. We thank Dr. Joan Massagué (MSKCC, NY, USA) for donating cell lines. We thank Dr. Gerhard Christofori (University of Basel) for comments on the manuscript, as well as all members of the Aceto lab for feedback and discussions. We thank Katja Eschbach and Elodie Burcklen from the Genomics Facility Basel (D-BSSE of the ETH Zürich) for generating sequencing libraries and performing next-generation sequencing and Dr. Elena Parmigiani for sharing reagents. We thank Dr. Gleb Turchinovich, Dr. Massimo Saini, and the members of the flow cytometer core (DBM of University of Basel) for performing flow cytometer analysis. We thank Pascal Lorentz for microscopy assistance and all members of the mouse core facility (DBM of University of Basel) for support with mouse experiments. We thank Drs. Katarzyna Buczak and Alexander Schmidt from the Proteomics Core Facility (Biozentrum of University of Basel) for mass spectrometry analysis. Calculations were performed at sciCORE (https://scicore.unibas.ch/) scientific computing center at the University of Basel. Research in the Aceto lab is supported by the European Research Council (678834 and 840636), the European Union (801159-B2B), the Swiss National Science Foundation (PP0P3_163938, PP00P3_190077, IZLIZ3_182962), the Swiss Cancer League (KFS-3811-02-2016, KLS-4222-08-2017, KLS-4834-08-2019), the Basel Cancer League (KLbB-4173-03-2017, KLbB-4763-02-2019), the two Cantons of Basel through the ETH Zürich (PMB-01-16), and the University of Basel, Switzerland. This study is also supported by Swiss National Science Foundation grants awarded to T.S. (179490) and to A.B. (182357).

AUTHOR CONTRIBUTIONS

C.D. and N.A. designed the study, performed the experiments, and drafted the manuscript. L.K. and T.S. performed immunofluorescence staining and confocal imaging. F.C.-G. performed the computational analysis. A.P.-S., K.S., and R.S. processed blood samples and mouse tissues and helped with all molecular biology procedures. B.M.S. performed CTC picking, single-cell RNA extraction, and amplification. N.D.M. and A.B. provided VEGFA-overexpressing vectors and input throughout the project. W.H. and O.B. provided support with microscopy. C.B. generated sequencing data. M.V., C.R., and W.P.W. provided patient samples and clinical input throughout the project. All authors have read, commented, and approved the manuscript in its final form.

DECLARATION OF INTERESTS

N.A. and C.D. are listed as inventors in patent application EP 19188215.8, "Angiogenesis promoting agents for prevention of metastatic cancer." N.A. is a paid consultant for companies with an interest in liquid biopsy.

Received: August 27, 2019
Revised: June 11, 2020
Accepted: August 12, 2020
Published: September 8, 2020

REFERENCES

Aceto, N., Bardia, A., Miyamoto, D.T., Donaldson, M.C., Wittner, B.S., Spencer, J.A., Yu, M., Pely, A., Engstrom, A., Zhu, H., et al. (2014). Circulating tumor cell clusters are oligoclonal precursors of breast cancer metastasis. Cell *158*, 1110–1122.

Aceto, N., Toner, M., Maheswaran, S., and Haber, D.A. (2015). En Route to Metastasis: Circulating Tumor Cell Clusters and Epithelial-to-Mesenchymal Transition. Trends Cancer *1*, 44–52.

Alix-Panabières, C., and Pantel, K. (2014). Challenges in circulating tumour cell research. Nat. Rev. Cancer *14*, 623–631.

Baba, Y., Nosho, K., Shima, K., Irahara, N., Chan, A.T., Meyerhardt, J.A., Chung, D.C., Giovannucci, E.L., Fuchs, C.S., and Ogino, S. (2010). HIF1A overexpression is associated with poor prognosis in a cohort of 731 colorectal cancers. Am. J. Pathol. *176*, 2292–2301.

Bos, P.D., Zhang, X.H., Nadal, C., Shu, W., Gomis, R.R., Nguyen, D.X., Minn, A.J., van de Vijver, M.J., Gerald, W.L., Foekens, J.A., and Massagué, J. (2009). Genes that mediate breast cancer metastasis to the brain. Nature *459*, 1005–1009.

Buffa, F.M., Harris, A.L., West, C.M., and Miller, C.J. (2010). Large meta-analysis of multiple cancers reveals a common, compact and highly prognostic hypoxia metagene. Br. J. Cancer *102*, 428–435.

Carmeliet, P., and Jain, R.K. (2011). Principles and mechanisms of vessel normalization for cancer and other angiogenic diseases. Nat. Rev. Drug Discov. *10*, 417–427.

Chen, X., Iliopoulos, D., Zhang, Q., Tang, Q., Greenblatt, M.B., Hatziapostolou, M., Lim, E., Tam, W.L., Ni, M., Chen, Y., et al. (2014). XBP1 promotes triple-negative breast cancer by controlling the HIF1α pathway. Nature *508*, 103–107.

Cheung, K.J., and Ewald, A.J. (2016). A collective route to metastasis: Seeding by tumor cell clusters. Science *352*, 167–169.

Cheung, K.J., Padmanaban, V., Silvestri, V., Schipper, K., Cohen, J.D., Fairchild, A.N., Gorin, M.A., Verdone, J.E., Pienta, K.J., Bader, J.S., and Ewald, A.J. (2016). Polyclonal breast cancer metastases arise from collective dissemination of keratin 14-expressing tumor cell clusters. Proc. Natl. Acad. Sci. USA *113*, E854–E863.

Chiron, M., Bagley, R.G., Pollard, J., Mankoo, P.K., Henry, C., Vincent, L., Geslin, C., Baltes, N., and Bergstrom, D.A. (2014). Differential antitumor activity of aflibercept and bevacizumab in patient-derived xenograft models of colorectal cancer. Mol. Cancer Ther. *13*, 1636–1644.

Coffelt, S.B., Kersten, K., Doornebal, C.W., Weiden, J., Vrijland, K., Hau, C.S., Verstegen, N.J.M., Ciampricotti, M., Hawinkels, L.J.A.C., Jonkers, J., and de

Visser, K.E. (2015). IL-17-producing γδ T cells and neutrophils conspire to promote breast cancer metastasis. Nature *522*, 345–348.

Comerford, K.M., Wallace, T.J., Karhausen, J., Louis, N.A., Montalto, M.C., and Colgan, S.P. (2002). Hypoxia-inducible factor-1-dependent regulation of the multidrug resistance (MDR1) gene. Cancer Res. *62*, 3387–3394.

Coutu, D.L., Kokkaliaris, K.D., Kunz, L., and Schroeder, T. (2018). Multicolor quantitative confocal imaging cytometry. Nat. Methods *15*, 39–46.

Donato, C., Szczerba, B.M., Scheidmann, M.C., Castro-Giner, F., and Aceto, N. (2019). Micromanipulation of Circulating Tumor Cells for Downstream Molecular Analysis and Metastatic Potential Assessment. J. Vis. Exp. (*147*)

Duda, D.G., Duyverman, A.M., Kohno, M., Snuderl, M., Steller, E.J., Fukumura, D., and Jain, R.K. (2010). Malignant cells facilitate lung metastasis by bringing their own soil. Proc. Natl. Acad. Sci. USA *107*, 21677–21682.

Elvidge, G.P., Glenny, L., Appelhoff, R.J., Ratcliffe, P.J., Ragoussis, J., and Gleadle, J.M. (2006). Concordant regulation of gene expression by hypoxia and 2-oxoglutarate-dependent dioxygenase inhibition: the role of HIF-1alpha, HIF-2alpha, and other pathways. J. Biol. Chem. *281*, 15215–15226.

Esposito, M., Guise, T., and Kang, Y. (2018). The Biology of Bone Metastasis. Cold Spring Harb. Perspect. Med. *8*, a031252.

Ferrara, N., Hillan, K.J., Gerber, H.P., and Novotny, W. (2004). Discovery and development of bevacizumab, an anti-VEGF antibody for treating cancer. Nat. Rev. Drug Discov. *3*, 391–400.

Ferrara, N., Mass, R.D., Campa, C., and Kim, R. (2007). Targeting VEGF-A to treat cancer and age-related macular degeneration. Annu. Rev. Med. *58*, 491–504.

Folkman, J. (1971). Tumor angiogenesis: therapeutic implications. N. Engl. J. Med. *285*, 1182–1186.

Forsythe, J.A., Jiang, B.H., Iyer, N.V., Agani, F., Leung, S.W., Koos, R.D., and Semenza, G.L. (1996). Activation of vascular endothelial growth factor gene transcription by hypoxia-inducible factor 1. Mol. Cell. Biol. *16*, 4604–4613.

Fujimura, A., Michiue, H., Cheng, Y., Uneda, A., Tani, Y., Nishiki, T., Ichikawa, T., Wei, F.Y., Tomizawa, K., and Matsui, H. (2013). Cyclin G2 promotes hypoxia-driven local invasion of glioblastoma by orchestrating cytoskeletal dynamics. Neoplasia *15*, 1272–1281.

Gerber, H.-P., Kowalski, J., Sherman, D., Eberhard, D.A., and Ferrara, N. (2000). Complete inhibition of rhabdomyosarcoma xenograft growth and neovascularization requires blockade of both tumor and host vascular endothelial growth factor. Cancer Res. *60*, 6253–6258.

Gilkes, D.M., Semenza, G.L., and Wirtz, D. (2014). Hypoxia and the extracellular matrix: drivers of tumour metastasis. Nat. Rev. Cancer *14*, 430–439.

Gkountela, S., Castro-Giner, F., Szczerba, B.M., Vetter, M., Landin, J., Scherrer, R., Krol, I., Scheidmann, M.C., Beisel, C., Stirnimann, C.U., et al. (2019). Circulating Tumor Cell Clustering Shapes DNA Methylation to Enable Metastasis Seeding. Cell *176*, 98–112.e114.

Gligorov, J., Doval, D., Bines, J., Alba, E., Cortes, P., Pierga, J.Y., Gupta, V., Costa, R., Srock, S., de Ducla, S., et al. (2014). Maintenance capecitabine and bevacizumab versus bevacizumab alone after initial first-line bevacizumab and docetaxel for patients with HER2-negative metastatic breast cancer (IMELDA): a randomised, open-label, phase 3 trial. Lancet Oncol. *15*, 1351–1360.

Goel, S., Duda, D.G., Xu, L., Munn, L.L., Boucher, Y., Fukumura, D., and Jain, R.K. (2011). Normalization of the vasculature for treatment of cancer and other diseases. Physiol. Rev. *91*, 1071–1121.

Gray, L.H., Conger, A.D., Ebert, M., Hornsey, S., and Scott, O.C. (1953). The concentration of oxygen dissolved in tissues at the time of irradiation as a factor in radiotherapy. Br. J. Radiol. *26*, 638–648.

Groppa, E., Brkic, S., Uccelli, A., Wirth, G., Korpisalo-Pirinen, P., Filippova, M., Dasen, B., Sacchi, V., Muraro, M.G., Trani, M., et al. (2018). EphrinB2/EphB4 signaling regulates non-sprouting angiogenesis by VEGF. EMBO Rep. *19*, e45054.

Hanahan, D., and Weinberg, R.A. (2011). Hallmarks of cancer: the next generation. Cell *144*, 646–674.

Harada, H., Kizaka-Kondoh, S., Itasaka, S., Shibuya, K., Morinibu, A., Shinomiya, K., and Hiraoka, M. (2007). The combination of hypoxia-response enhancers and an oxygen-dependent proteolytic motif enables real-time imaging of absolute HIF-1 activity in tumor xenografts. Biochem. Biophys. Res. Commun. *360*, 791–796.

Harper, S.J., and Bates, D.O. (2008). VEGF-A splicing: the key to anti-angiogenic therapeutics? Nat. Rev. Cancer *8*, 880–887.

Harrop, G.A., Jr. (1919). The oxygen and carbon dioxide content of arterial and of venous blood in normal individuals and in patients with anemia and heart disease. J. Exp. Med. *30*, 241–257.

Hicklin, D.J., and Ellis, L.M. (2005). Role of the vascular endothelial growth factor pathway in tumor growth and angiogenesis. J. Clin. Oncol. *23*, 1011–1027.

Höckel, M., and Vaupel, P. (2001). Biological consequences of tumor hypoxia. Semin. Oncol. *28*, 36–41.

Jain, R.K. (2005). Normalization of tumor vasculature: an emerging concept in antiangiogenic therapy. Science *307*, 58–62.

Jain, R.K. (2013). Normalizing tumor microenvironment to treat cancer: bench to bedside to biomarkers. J. Clin. Oncol. *31*, 2205–2218.

Jayson, G.C., Kerbel, R., Ellis, L.M., and Harris, A.L. (2016). Antiangiogenic therapy in oncology: current status and future directions. Lancet *388*, 518–529.

Kang, Y., Siegel, P.M., Shu, W., Drobnjak, M., Kakonen, S.M., Cordón-Cardo, C., Guise, T.A., and Massagué, J. (2003). A multigenic program mediating breast cancer metastasis to bone. Cancer Cell *3*, 537–549.

Lachat, P., Shaw, P., Gebhard, S., van Belzen, N., Chaubert, P., and Bosman, F.T. (2002). Expression of NDRG1, a differentiation-related gene, in human tissues. Histochem. Cell Biol. *118*, 399–408.

Lakhal, S., Talbot, N.P., Crosby, A., Stoepker, C., Townsend, A.R., Robbins, P.A., Pugh, C.W., Ratcliffe, P.J., and Mole, D.R. (2009). Regulation of growth differentiation factor 15 expression by intracellular iron. Blood *113*, 1555–1563.

Lang, I., Brodowicz, T., Ryvo, L., Kahan, Z., Greil, R., Beslija, S., Stemmer, S.M., Kaufman, B., Zvirbule, Z., Steger, G.G., et al.; Central European Cooperative Oncology Group (2013). Bevacizumab plus paclitaxel versus bevacizumab plus capecitabine as first-line treatment for HER2-negative metastatic breast cancer: interim efficacy results of the randomised, open-label, non-inferiority, phase 3 TURANDOT trial. Lancet Oncol. *14*, 125–133.

Li, H., Takayama, K., Wang, S., Shiraishi, Y., Gotanda, K., Harada, T., Furuyama, K., Iwama, E., Ieiri, I., Okamoto, I., and Nakanishi, Y. (2014). Addition of bevacizumab enhances antitumor activity of erlotinib against non-small cell lung cancer xenografts depending on VEGF expression. Cancer Chemother. Pharmacol. *74*, 1297–1305.

Lizama-Manibusan, B.N., Klein, S., McKenzie, J.R., Cliffel, D.E., and McLaughlin, B. (2016). Analysis of a Nitroreductase-Based Hypoxia Sensor in Primary Neuronal Cultures. ACS Chem. Neurosci. *7*, 1188–1191.

Lundgren, K., Nordenskjöld, B., and Landberg, G. (2009). Hypoxia, Snail and incomplete epithelial-mesenchymal transition in breast cancer. Br. J. Cancer *101*, 1769–1781.

Macaulay, I.C., Haerty, W., Kumar, P., Li, Y.I., Hu, T.X., Teng, M.J., Goolam, M., Saurat, N., Coupland, P., Shirley, L.M., et al. (2015). G&T-seq: parallel sequencing of single-cell genomes and transcriptomes. Nat. Methods *12*, 519–522.

Massagué, J., and Obenauf, A.C. (2016). Metastatic colonization by circulating tumour cells. Nature *529*, 298–306.

Miller, K., Wang, M., Gralow, J., Dickler, M., Cobleigh, M., Perez, E.A., Shenkier, T., Cella, D., and Davidson, N.E. (2007). Paclitaxel plus bevacizumab versus paclitaxel alone for metastatic breast cancer. N. Engl. J. Med. *357*, 2666–2676.

Minn, A.J., Gupta, G.P., Siegel, P.M., Bos, P.D., Shu, W., Giri, D.D., Viale, A., Olshen, A.B., Gerald, W.L., and Massagué, J. (2005). Genes that mediate breast cancer metastasis to lung. Nature *436*, 518–524.

Misteli, H., Wolff, T., Füglistaler, P., Gianni-Barrera, R., Gürke, L., Heberer, M., and Banfi, A. (2010). High-throughput flow cytometry purification of

transduced progenitors expressing defined levels of vascular endothelial growth factor induces controlled angiogenesis in vivo. Stem Cells *28*, 611–619.

Mucaj, V., Shay, J.E., and Simon, M.C. (2012). Effects of hypoxia and HIFs on cancer metabolism. Int. J. Hematol. *95*, 464–470.

Mujagic, E., Gianni-Barrera, R., Trani, M., Patel, A., Gürke, L., Heberer, M., Wolff, T., and Banfi, A. (2013). Induction of aberrant vascular growth, but not of normal angiogenesis, by cell-based expression of different doses of human and mouse VEGF is species-dependent. Hum. Gene Ther. Methods *24*, 28–37.

Ozawa, C.R., Banfi, A., Glazer, N.L., Thurston, G., Springer, M.L., Kraft, P.E., McDonald, D.M., and Blau, H.M. (2004). Microenvironmental VEGF concentration, not total dose, determines a threshold between normal and aberrant angiogenesis. J. Clin. Invest. *113*, 516–527.

Pagès, G., and Pouysségur, J. (2005). Transcriptional regulation of the Vascular Endothelial Growth Factor gene–a concert of activating factors. Cardiovasc. Res. *65*, 564–573.

Peinado, H., Zhang, H., Matei, I.R., Costa-Silva, B., Hoshino, A., Rodrigues, G., Psaila, B., Kaplan, R.N., Bromberg, J.F., Kang, Y., et al. (2017). Pre-metastatic niches: organ-specific homes for metastases. Nat. Rev. Cancer *17*, 302–317.

Picelli, S., Björklund, A.K., Faridani, O.R., Sagasser, S., Winberg, G., and Sandberg, R. (2013). Smart-seq2 for sensitive full-length transcriptome profiling in single cells. Nat. Methods *10*, 1096–1098.

Quail, D.F., and Joyce, J.A. (2013). Microenvironmental regulation of tumor progression and metastasis. Nat. Med. *19*, 1423–1437.

Ragnum, H.B., Vlatkovic, L., Lie, A.K., Axcrona, K., Julin, C.H., Frikstad, K.M., Hole, K.H., Seierstad, T., and Lyng, H. (2015). The tumour hypoxia marker pimonidazole reflects a transcriptional programme associated with aggressive prostate cancer. Br. J. Cancer *112*, 382–390.

Rankin, E.B., and Giaccia, A.J. (2016). Hypoxic control of metastasis. Science *352*, 175–180.

Robert, N.J., Diéras, V., Glaspy, J., Brufsky, A.M., Bondarenko, I., Lipatov, O.N., Perez, E.A., Yardley, D.A., Chan, S.Y., Zhou, X., et al. (2011). RIBBON-1: randomized, double-blind, placebo-controlled, phase III trial of chemotherapy with or without bevacizumab for first-line treatment of human epidermal growth factor receptor 2-negative, locally recurrent or metastatic breast cancer. J. Clin. Oncol. *29*, 1252–1260.

Said, H.M., Safari, R., Al-Kafaji, G., Ernestus, R.I., Löhr, M., Katzer, A., Flentje, M., and Hagemann, C. (2017). Time- and oxygen-dependent expression and regulation of NDRG1 in human brain cancer cells. Oncol. Rep. *37*, 3625–3634.

Samanta, D., Gilkes, D.M., Chaturvedi, P., Xiang, L., and Semenza, G.L. (2014). Hypoxia-inducible factors are required for chemotherapy resistance of breast cancer stem cells. Proc. Natl. Acad. Sci. USA *111*, E5429–E5438.

Semenza, G.L. (1998). Hypoxia-inducible factor 1: master regulator of O2 homeostasis. Curr. Opin. Genet. Dev. *8*, 588–594.

Semenza, G.L. (2010). Defining the role of hypoxia-inducible factor 1 in cancer biology and therapeutics. Oncogene *29*, 625–634.

Shibata, T., Giaccia, A.J., and Brown, J.M. (2000). Development of a hypoxia-responsive vector for tumor-specific gene therapy. Gene Ther. *7*, 493–498.

Stylianopoulos, T., Munn, L.L., and Jain, R.K. (2018). Reengineering the Tumor Vasculature: Improving Drug Delivery and Efficacy. Trends Cancer *4*, 258–259.

Szczerba, B.M., Castro-Giner, F., Vetter, M., Krol, I., Gkountela, S., Landin, J., Scheidmann, M.C., Donato, C., Scherrer, R., Singer, J., et al. (2019). Neutrophils escort circulating tumour cells to enable cell cycle progression. Nature *566*, 553–557.

Varia, M.A., Calkins-Adams, D.P., Rinker, L.H., Kennedy, A.S., Novotny, D.B., Fowler, W.C., Jr., and Raleigh, J.A. (1998). Pimonidazole: a novel hypoxia marker for complementary study of tumor hypoxia and cell proliferation in cervical carcinoma. Gynecol. Oncol. *71*, 270–277.

Vasudev, N.S., and Reynolds, A.R. (2014). Anti-angiogenic therapy for cancer: current progress, unresolved questions and future directions. Angiogenesis *17*, 471–494.

von Baumgarten, L., Brucker, D., Tirniceru, A., Kienast, Y., Grau, S., Burgold, S., Herms, J., and Winkler, F. (2011). Bevacizumab has differential and dose-dependent effects on glioma blood vessels and tumor cells. Clin. Cancer Res. *17*, 6192–6205.

Winter, S.C., Buffa, F.M., Silva, P., Miller, C., Valentine, H.R., Turley, H., Shah, K.A., Cox, G.J., Corbridge, R.J., Homer, J.J., et al. (2007). Relation of a hypoxia metagene derived from head and neck cancer to prognosis of multiple cancers. Cancer Res. *67*, 3441–3449.

Xiong, G., Stewart, R.L., Chen, J., Gao, T., Scott, T.L., Samayoa, L.M., O'Connor, K., Lane, A.N., and Xu, R. (2018). Collagen prolyl 4-hydroxylase 1 is essential for HIF-1α stabilization and TNBC chemoresistance. Nat. Commun. *9*, 4456.

STAR★METHODS

KEY RESOURCES TABLE

REAGENT or RESOURCE	SOURCE	IDENTIFIER
Antibodies		
EpCAM-AF488	Cell Signaling	Cat# CST5198; RRID: AB_10692105
HER2-AF488	BioLegend	Cat# 324410; RRID: AB_2099256
EGFR-FITC	GeneTex	Cat# GTX11400; RRID: AB_368217
CD45-AF647 (anti mouse)	BioLegend	Cat# 103124, RRID: AB_493533
Anti-HIF1α	Novus	Cat# NB100-449, RRID: AB_10001045
Chemicals, Peptides, and Recombinant Proteins		
Deferoxamine	Sigma	Cat# D9533
Ephrin-B2-hFC chimera	R&D Biosystem	Cat# 496-EB-200
Critical Commercial Assays		
HypoxiaRed	Enzo Life technologies	ENZ-51042-K500
Deposited Data		
RNA sequencing	This paper and Szczerba et al., 2019	GSE126669
Experimental Models: Cell Lines		
BR16 CTC-derived	Aceto lab, University of Basel	n/a
MDA-MB-231 LM2	Massague lab, MSKCC	n/a
4T1	ATCC	Cat# ATCC® CRL-2539
HEK293T	Banfi lab, University Hospital Basel	n/a
HUVEC	Banfi lab, University Hospital Basel	n/a
MAEC	Banfi lab, University Hospital Basel	n/a
Experimental Models: Organisms/Strains		
NOD.Cg-Prkdcscid Il2rgtm1Wjl/SzJ	The Jackson Laboratory	Cat# 5557
Biological Samples		
Human metastatic breast cancer patient blood samples	University Hospital Basel	BR61

RESOURCE AVAILABILITY

Lead contact

Further information and requests for resources and reagents should be directed to and will be fulfilled by the Lead Contact, Nicola Aceto (Nicola.Aceto@unibas.ch).

Materials availability

The HIF1α activity reporter generated in this study is available from the Lead Contact upon Materials Transfer Agreement.

Data and code availability

Software specification

Data analysis of RNA-seq data after quantification, differential expression, and survival analysis was run in R v3.5 and bioconductor v3.8. Data visualization and statistical analyses were performed in GraphPad Prism v7 (GraphPad Software, San Diego, CA), R, ggplot2 and ComplexHeatmap.

Data and materials availability

RNA sequencing data have been deposited to Gene Expression Omnibus (GEO, NCBI) with accession number GSE126669.

EXPERIMENTAL MODEL AND SUBJECT DETAILS

Human blood samples collection

Patient blood specimens were obtained at the University Hospital Basel through the study protocols (EKNZ BASEC 2016-00067 and EK 321/10), approved by the local ethics committee (EKNZ, Ethics Committee northwest/central Switzerland). The patients involved were characterized by having invasive breast cancer, high tumor load and progressive disease. In particular, breast cancer patient BR61, female of age 63 at time of blood withdrawal, was characterized by having a ER-positive, PR-negative and HER2-negative disease at primary tumor diagnosis, and later developed bone, lymph node, soft tissue, brain, adrenal gland and pancreatic metastases at the time of CTC isolation. BR61 donated 7.5 –15ml blood in EDTA vacutainers at multiple time points during disease progression, upon written informed consent.

Mouse blood samples collection

All mouse experiments were carried out in compliance with institutional and cantonal guidelines (approved mouse protocol #2781, cantonal veterinary office of Basel-City). NOD/scid GAMMA (NSG) mice were purchased from Jackson Laboratory and kept in pathogen-free conditions specified by the University of Basel and cantonal veterinary office of Basel-City. Mouse blood was retrieved via cardiac puncture of NSG female mice (age range 8-12 weeks), and up to 1 mL of blood was collected.

Cell lines

MDA-MB-231-LM2 (LM2) human triple negative breast cancer cell line was obtained from Dr. Joan Massagué, MSKCC, NY, USA. CTC-derived BR16 cells were generated and cultured from the corresponding patient as previously described (Gkountela et al., 2019). 4T1 murine breast cancer cells were purchased from ATCC (4T1 ATCC® CRL-2539). HEK293T Phoenix packaging cells, Human umbilical cord endothelial cells (HUVEC) and Mouse aortic endothelial cells (MAEC) were kindly donated by Dr. Andrea Banfi, University Hospital Basel, Switzerland.

METHOD DETAILS

Cell culture

LM2, 4T1, and HEK293T cells were grown in DMEM F-12 high glucose (GIBCO, 11330-057) supplemented with 10% heat-inactivated FBS (GIBCO, 10500064) and 1% antimycotic/antibiotic (GIBCO, 15240-062) in a humidified incubator at 37 °C with 20% O_2 and 5% CO_2. BR16 cells were grown as suspension cultures in RPMI medium (GIBCO, 52400-025) supplemented with 1X B27 (GIBCO, 17504-044), 1% antimycotic/antibiotic, 20 ng/ml human recombinant Fibroblast Growth Factor (FGF; Peprotech, 100-18B) and 20 ng/ml human recombinant Epidermal Growth Factor (EGF; Invitrogen, PHG0313) in a humidified incubator at 37 °C with 5% O_2 and 5% CO_2, using ultra-low attachment plates (Sarstedt, 83.3920.500). HUVEC and MAEC were grown in endothelial cell growth medium 2 (ready-to-use) (Promocell, C-22011) supplemented with 1% antimycotic/antibiotic. LM2, 4T1 and BR16 cells were stably transduced with lentiviral vectors expressing UBC_GFP-T2A-Firefly Luciferase (GFP/Luc) (System Biosciences, BLIV200PA-1-SBI) or ready-to-use virus EF1α_Firefly Luciferase-T2A-mCherry (mCherry/Luc) (Biosettia, GlowCell-15-10).

HIF1α activity reporter

The HIF1α activity reporter (HIF1α reporter) was purchased from Genecopoeia upon providing the exact nucleotide sequence. The human hypoxia response element (HRE) of the human *VEGFA* gene (“5′ - CCACAGTGCATACGTGGGCTCCAACAGGTCCTCTT −3′”) (Harada et al., 2007) is followed by a CMV minimal promoter (CMVmp) (Shibata et al., 2000) and by an enhanced yellow fluorescent protein (eYFP) sequence within a lentiviral vector. Transduced cells were selected with 5 μg/ml Puromycin (Invitrogen, ant-pr-1) for 5 days (4T1) or 0.5 μg/ml for 5 days (LM2) or 15 days (BR16), respectively. Treatment with Deferoxamine (DFO; Sigma, D9533) 500 μM was used to induce the stabilization of HIF1α in LM2, 4T1 and BR16 cells, for 4, 8 and 15 hours, respectively. Alternatively, HIF1α induction was achieved using the humidified hypoxia chamber (Biospherix, ProOx 110) at 0.1% O_2. Anti-HIF1α (Novus, NB100-449) antibodies were used to confirm HIF1α induction through western blot, with anti-GAPDH antibody (Cell Signaling, 2118S) as loading control.

Live imaging of HIF1α reporter

LM2, 4T1 and BR16 mCherry/Luc cells, expressing the HIF1α reporter, were seeded into coated (LM2 and 4T1) or uncoated (BR16) imaging chambers (Ibidi, 80826 and 80821), respectively. Following treatment with DFO, Diethyl Fumarate (DF; Sigma, D95654), Dimethyl Succinate (DS; Sigma, 73605), Rotenone (RT; Sigma, R8875) or Hydrogen peroxide (H_2O_2; Sigma, H1009), cells within chambers were cultured under the humidified live imaging box of the microscope Leica DMi8, at 37°C and 20% O_2. For live imaging experiments requiring hypoxia, cells within chambers were cultured at 5% O_2 or 0.1% O_2.

hHIF1α, hVEGFA and mVegfa knockdown

LM2 and BR16 cells were stably transduced with doxycycline (Dox)-inducible shRNAs, targeting the Open Reading Frame (ORF) of human *HIF1α (*5′ - AAAGATATGATTGTGTCTC - 3′and 5′ - TGCATCTCGAGACTTTTCT - 3′), (Dharmacon, TRIPZ®). LM2 and 4T1 cells were stably transduced with Dox-inducible shRNAs targeting ORF of human *VEGFA (5′-CAGGGTCTCGATTGGATGG - 3′, 5′ - AGTAGCTGCGCTGATAGAC - 3′),* or mouse *Vegfa* (5′-ACCGCCTTGGCTTGTCACA - 3′, 5′ - ACCGCCTTGGCTTGTCACA - 3′) (Dharmacon, SMART®), respectively. The transduced cells were selected using 0.5 - 5 μg/ml puromycin and subsequently sorted, upon treatment with 0.1 μg/ml doxycycline (Dox; Sigma, D9891) for 2 days, for the highest expression of the shRNA-coupled fluorophore (TurboGFP or TurboRFP). h*HIF1α* knockdown was measured by western blot as described above or by qPCR using previously described primers (Chen et al., 2014). Anti-HIF2α (Novus, NB100-122SS) antibodies were used to measure HIF2α protein level by western blot. h*VEGFA* and m*Vegfa* knockdown was measured by qPCR using previously described primers (Chen et al., 2014; Mujagic et al., 2013). h*GAPDH* (forward primer: 5′ - GAAGGTGAAGGTCGGAGTCAAC - 3′, reverse primer: 5′ - CAGAGTTAAAAG CAGCCCTGGT - 3′) or m*Gapdh* (forward primer: 5′ - AATGGTGAAGGTCGGTGTG - 3′, and reverse primer: 5′ -GTGGAGTCATACTG GAACATGTAG - 3′) were used as load controls. Treatment with DFO 500 μM was used to induce the stabilization of HIF1α in LM2, 4T1 and BR16 cells, for 4, 8 and 15 hours, respectively, upon 5 days of treatment with 0.1 μg/ml Dox.

$mVEGFA_{164}$-tCD8a overexpression

$mVEGFA_{164}$-mCD8aTr and mCD8aTr only were transduced in LM2 and 4T1 mCherry/Luc as previously described (Mujagic et al., 2013). Clonal populations were derived from single cells, obtained through single-cell sorting with BD FACS ARIA in 96-well plates. Successfully growing clones were expanded and analyzed for CD8aTr expression at the CytoFLEX (Beckman Coulter Life sciences, V-B-R series) upon staining with anti-CD8aTr APC (Biolegend, 100712) or isotype control Rat IgG2a (Biolegend, 400511) as previously described (Misteli et al., 2010). Clones were further selected based on morphology and stable expression of CD8aTr over multiple *in vitro* culture passages.

EphB4 western blot analysis

HUVEC, LM2, BR16, MAEC and 4T1 cells were incubated in the presence of 1 μg/ml of recombinant mouse Ephrin-B2-hFC chimera (R&D Biosystem, 496-EB-200) or ChromPure IgG hFC fragment (Jackson Immuno research, 009-000-008) for 3 hours and subsequently lysed. Anti-hEphB4 (R&D systems, AF3038-SP) and anti-mEphB4 (R&D systems, AF446-SP) antibodies were used to confirm EphB4 induction through western blot, with anti-GAPDH antibody as loading control.

Mouse experiments

Orthotopic injection was performed between the second and third mammary gland of adult female mice (age range 8-12 weeks) with either $1x10^6$ LM2, $1x10^6$ BR16 or $0.25x10^6$ 4T1 cells, expressing the fluorescent construct GFP/Luc or mCherry/Luc. Cells were inoculated in 50% Cultrex Path Clear Reduced Growth Factor Basement Membrane Extract (R&D Biosystems, 3533-010-02) and 50% PBS. In mice injected with cells carrying a dox-inducible construct, water containing 0.5 mg/ml Dox (Sigma, D9891-25G) and 5% sucrose (Sigma, S9378) was administered 3 times a week upon tumor formation and for a maximum of 3 months. Injection of 0.02 mg in PBS of recombinant mEphrin-B2-hFC chimera or ChromPure IgG hFC fragment was performed intra-peritoneal (i.p.) and with a frequency of twice per week. Injection of 25 mg/Kg Bevacizumab in PBS (Genentech, Avastin®) or 26.25 mg/Kg Paclitaxel in PBS (Bristol-Myers Squibb, Taxol®) or Ultra-LEAF purified human IgG1 Isotype control (Biolegend, 403502) was performed i.p. and with a frequency of twice per week. Injection of 15 mg/Kg Paclitaxel in PBS (Bristol-Myers Squibb, Taxol®) was performed i.p. once a week. Bevacizumab and Paclitaxel were obtained from the Pharmacy of the University Hospital Basel, under permit #RL0004-V07-B02.

Metastatic index and organ fixation

Mice bearing GFP/Luc or mCherry/Luc tumors were subcutaneously (s.c.) injected with 3 mg D-Firefly-Luciferin (Gold Bio, LUCK-5G). After 10 minutes, bioluminescent images of the full mouse were taken at IVIS Lumina LT (Perkin Elmer). After euthanasia and within 20 minutes from the injection of luciferin, primary tumor and metastatic organs were imaged separately. Metastatic index was calculated as the ratio of the total flux in photons per second (Ph/s) of the metastatic organ over the primary tumor. Sample exclusion is applied to metastatic index greater than 1.3, mostly due to imprecise measurement as a consequence to high primary tumor necrosis. Primary tumors and metastatic organs were fixed in PFA-Lysine-Phosphate buffer (4% PFA, 0.2 M L-Lysine, 0.2% $NaIO_3$ and 0.1 M Phosphate buffer, pH 7.4 – 0.2 M NaH_2PO_4 and 0.2 M H_2HPO_4) O/N at 4°C. Subsequently, organs were incubated in 30% sucrose for 6 hours before O.C.T. embedding.

CTC capture and quantification

Patient-derived CTCs were enriched on the Parsortix Cell Separation Cassette (GEN3D6.5, ANGLE) within 1 hour of blood draw. In-cassette staining was performed with the antibody cocktail for anti-human EpCAM-AF488 (Cell Signaling, CST5198), anti-human HER2-AF488 (BioLegend, 324410) and anti-human EGFR-FITC (GeneTex, GTX11400). For mouse-derived CTCs capture, mice were anaesthetized using isoflurane and blood was drawn from the central circulation through cardiac puncture or from the tumor draining vessel. Blood was processed immediately on the Parsortix system for CTCs enrichment. For all xenograft models with

GFP/Luc, mCherry/Luc or dox-inducible sh-RNA reporters, CTCs were directly quantified in cassette using their fluorescence signal. In-cassette staining for hypoxic status was performed with HypoxiaRed (Enzo Life technologies, ENZ-51042-K500) in the presence of 1% BSA (Sigma, A8412) in PBS. For the HIF1α reporter/HypoxiaRed correlation analysis and the *in vitro* validation of the dye, LM2 or BR16 cells were stained for the HypoxiaRed according to the manufacturer protocol. Quantification of mouse-derived CTCs with HIF1α reporter or HypoxiaRed-stained CTCs was achieved by releasing the CTCs from the Parsortix system into a PBS solution and by analyzing the cell suspension through ImageStreamX Mark II (Amnis, Luminex). In particular, all the events between 13-100 μm diameter were analyzed with 40x objective and at slow flow rate for the acquisition of images. The 405, 488, 561 and side scatter (SSC) lasers were used. GFP/Luc or eYFP were acquired on Channel 2 (532/56), mCherry/Luc and HypoxiaRed on channel 4 (628/69). Analysis was performed at the IDEAS® software (Luminex, v6.0). Final graphs were created with FlowJo v10.

3D volumes and blood vessel functionality analysis

Mice bearing LM2, 4T1 or BR16 mCherry/Luc tumors expressing the HIF1α reporter were sacrificed at week 5, 3 or month 6 respectively, immediately after intra-peritoneal (i.p.) injection of 1.2 mg of Pimonidazole (Hypoxyprobe, HP-500mg) and intra-venous (i.v.) injection of 1 mg of Dextran-Biotin 70 kDa (Thermo Fisher, D1957), 1 hour and 15 minutes before the experiment termination, respectively. Tissue sections were prepared, stained, and imaged as previously described (Coutu et al., 2018). Primary tumors were fixed for 24 hours in 4% PFA at 4°C. Derived tissues were embedded in 4% low-gelling temperature agarose (Sigma, A9414) and subsequently sectioned (50-100 μm thick sections) using the Leica VT1200 S vibratome. For the IF staining, all protocol steps were performed at room temperature (RT) with permeabilization for a minimum of 2 hours followed by an O/N incubation with primary antibodies against GFP (Novus Biologicals, NB600-308), Pimonidazole-Red549 (Hypoxyprobe, Red549-Mab), human pan-Cytokeratin (7, 8, 18, 19) (Miltenyi Biotec, 130-112-743), and mouse CD31 (R&D, AF3628). Secondary antibodies against goat IgG-CF405 (Biotium, 20416), goat IgG-AF488 (Thermo Fisher, A-11055), goat IgG-DyLight 549 (Abcam, ab96933), rabbit IgG-CF405 (Biotium, 20420), mouse IgG-AF647 (Thermo Fisher, A-31571), human IgG-AF488 (Jackson Immuno Research, 709-545-149), human IgG-Cy3 (Jackson Immuno Research, 709-165-149), streptavidin-AF555 (Thermo Fisher, S32355), streptavidin-AF549 (Thermo Fisher, S32356), streptavidin-AF405 (Thermo Fisher, AF446-SP) were incubated for 2 hours after extensive washings. 3D volumes were constructed using Imaris (Bitplane, v9). Surface rendering was created for all the channels individually (mCherry or hCK, Pimonidazole, eYFP, CD31, Dextran). Area and volume of the individual surfaces were calculated with the Imaris "Measurement Pro" package. Channels were masked for "voxels out equal to 0" for colocalizing voxels of the respective channels, and with "voxels in equal to 0" for non-colocalizing voxels of the channels. Surface rendering of the masked channels was constructed to further calculate the area or volume of colocalizing channels.

Assessment of metastatic potential of hypoxic and normoxic CTC clusters

CTCs from mice bearing LM2-mCherry/Luc or BR16 tumors and expressing the HIF1α reporter were enriched with the Parsortix device, stained for mouse CD45-AF647 (Biolegend, 103124) and later released in a PBS solution, as described above. The CTC suspension was then micromanipulated using CellCelector® (ALS) and a 50 μm glass capillary was used to isolate CTC clusters from the CTC suspension. The total number of cells (in clusters or single cell form) was counted and injected through the tail vein of NSG tumor-free female recipients. BR16-mCherry/Luc cells, expressing the HIF1α reporter, were cultured in a humidified hypoxia chamber at 0.1% O_2 for four days before sorting. A control dish was cultured in a humidified incubator at 20% O_2 for four days before sorting. At day four, cells were collected and sorted at the BD Influx sorter at five pounds per square inch (psi) and with a 200 μm nozzle to preserve the integrity of both single and clustered cells. Equal numbers of eYFP-positive or eYFP-negative cells (in a cluster form) were injected through the tail vein of NSG tumor-free female recipients. I.v. injected mice were monitored weekly through non-invasive bioluminescence imaging and sacrificed when showing signs of distress.

CTC isolation and RNA Sequencing

Single cells or CTC clusters were isolated using CellCelector® based on the color combination of interest and deposited into individual tubes (Corning Axygen®, PCR-02-L-C) containing 2.5 μL RLT Plus lysis buffer (QIAGEN, 1053393) and 1U/μl SUPERase® In RNase Inhibitor (Invitrogen, AM2694) (Donato et al., 2019). Samples were immediately frozen on dry ice and kept at −80°C until further processing. Following previously published protocol for parallel DNA and RNA sequencing from individual cells (Macaulay et al., 2015), transcriptomes of lysed cells were separated and amplified according to the Smart-Seq2 (Picelli et al., 2013). Subsequently, libraries were prepared with Nextera XT (Illumina) and sequenced on NextSeq75 single read for RNA.

Mass spectrometry using tandem mass tags

Primary tumors from mice bearing LM2-mCherry/Luc tumors and expressing the HIF1α reporter were manually dissociated, digested with 0.1 μg/ml of Collagenase Type IV (Sigma Aldrich, C5138-1G) and 0.5 μg/ml DNase I (Roche, 11284932001) for 30' at 37°C, and purified using the Dead cell removal kit (Miltenyi Biotec, 130-090-101). mCherry/Luc positive cells were sorted based on the expression of the HIF1α reporter and classified as hypoxic (eYFP-positive) or normoxic (eYFP-negative). One million sorted cells were pelleted, washed twice with PBS and snap-frozen. CTCs from mice bearing LM2-mCherry/Luc tumors and expressing the HIF1α reporter were enriched, stained with anti-human CD298 PE (Biolegend, 341704) and anti-mouse CD45 AF647 and sorted in single CTCs and CTC clusters based on the expression of the HIF1α reporter and classified as hypoxic (eYFP-positive) or normoxic

(eYFP-negative). Sorted cells were pelleted, washed twice with PBS and snap-frozen. Cells were lysed in 8M Urea (Sigma), 0.1M ammonium bicarbonate in presence of phosphatase inhibitors (Sigma, P5726 and P0044) using strong ultra-sonication (Bioruptor, 10 cycles, 30 s on/off, Diagenode, Belgium). Proteins were reduced with 5 mM TCEP for 60 min at 37°C and alkylated with 10 mM chloroacetamide for 30 min at 37°C. Urea was diluted with 100 mM ammonium bicarbonate to the final concentration of 1.6M and proteins were digested by with sequencing-grade modified trypsin (1/50, w/w; Promega, Madison, Wisconsin) overnight at 37°C. Samples were then acidified with 5% TFA and peptides were desalted on C18 reversed-phase spin columns according to the manufacturer's instructions (Macrospin, Harvard Apparatus). 25 μg of peptides were labeled with tandem mass isobaric tags (TMT 10-plex, Thermo Fisher Scientific) according to the manufacturer's instructions. To control for ratio distortion, a peptide calibration mixture consisting of six standard peptide mix were added to each sample prior TMT labeling. After labeling, TMT peptides were pooled and again desalted on C18 reversed-phase spin columns. TMT-labeled peptides were fractionated by high-pH reversed phase separation using a XBridge Peptide BEH C18 column (3,5 μm, 130 A, 1 mm x 150 mm, Waters) on an Agilent 1260 Infinity HPLC system. Peptides were loaded on a column in ammonium formate (20 mM, pH 10) in water and eluted using a two-step linear gradient starting from 2% to 10% in 5 minutes and then to 50% (v/v) 90% acetonitrile / 10% ammonium formate (20 mM, pH 10) over 55 minutes at a flow rate of 42 μl/min. In total 36 fractions were collected and pooled into 12 fractions. 1 μg of peptides were processed for LC-MS. Chromatographic separation of peptides was carried out using an EASY nano-LC 1000 system (Thermo Fisher Scientific), equipped with a heated RP-HPLC column (75 μm x 37 cm) packed in-house with 1.9 μm C18 resin (Reprosil-AQ Pur, Dr. Maisch). Peptides were separated using a stepwise gradient ranging from 95% solvent A (0.15% formic acid, 2% acetonitrile) and 5% solvent B (80% acetonitrile, 20% water, 0.15% formic acid) to 45% solvent B over 120 minutes at a flow rate of 200 nl/min. Mass spectrometry analysis was performed on QExactive mass spectrometer equipped with a nano-electrospray ion source (both Thermo Fisher Scientific). Each MS1 scan was followed by high-collision-dissociation (HCD) of the 10 most abundant precursor ions with dynamic exclusion for 30 s. For MS1, 3e6 ions were accumulated in the Orbitrap cell and scanned at a resolution of 120,000 FWHM (at 200 m/z). MS2 scans were acquired at a target setting of 1e5 ions, accumulation time of 100 ms and a resolution of 30,000 FWHM (at 200 m/z). The normalized collision energy was set to 35%, the mass isolation window was set to 1.1 m/z and one microscan was acquired for each spectrum.

Immunofluorescent staining of blood vessels and hypoxic cells

7 μm-thick frozen slices were blocked for 30 minutes in 0.1% Gelatin buffer (Sigma, G9391) for LM2 and 4T1, or 10% Donkey serum buffer (Millipore, S30) for BR16. Primary antibodies for mouse CD31 (R&D, AF3628), Pimonidazole (Hypoxyprobe, Red549-Mab, FITC-Mab, Pacific Blue-Mab), and human pan-Cytokeratin (i.e., cytokeratins 7, 8, 18, 19) (Miltenyi Biotec, 130-112-743) were incubated O/N at 4°C. Secondary antibodies against rabbit IgG-AF647 (Invitrogen, A31573), FITC IgG-CF633 (Scientific Laboratory supply, SAB 4600145), and goat IgG-AF633 (Thermo Fischer, A-21082) were incubated, after washing in PBS, for 1 hour at RT. Slides were mounted with Vectashield Hard set with Dapi (Vectashield, VC-H-1400-L010). Slides were scanned at the Zeiss Axio Imager Z2 with a 20x dry objective. CD31 quantification was performed with Fiji (v2) using the plugin "color pixel counter" of the CD31 over the total tumor background color area (e.g., mCherry or GFP). Pimonidazole quantification was performed with Fiji using the "colocalization threshold" analysis tool of the total tumor background color over the pimonidazole.

Pimonidazole or Ki67 (Abcam, ab15580) staining on sorted CTCs was performed using Cytospin (500 rpm, 3 minutes), immediate fixation in 4% PFA for 12 minutes and staining as described above. Slides were imaged at Leica SP5 confocal microscope with a 40x oil objective.

NDRG1 immunofluorescence and western blot analysis

O.C.T.-embedded consecutive sections of LM2-mCherry/Luc tumors expressing the HIF1α reporter were stained NDRG1 (Cell Signaling, 9485). NDRG1 expression in hypoxic conditions was assessed by incubating LM2-mCherry/Luc cells in the presence of 500 μM DFO or in hypoxia 0.1% O_2 for 15 hours before lysis. Anti-NDRG1 (Cell signaling, 9395) was used to detect NDRG1 protein and anti-alpha Tubulin (Sigma Aldrich, T9026) was used as loading control. LM2 cells were stably transduced with Dox-inducible shRNAs targeting ORF of human *NDRG1 (5′- GAAAGAATCAAGGAGG - 3′, 5′ - GGAAAGAATCAAGGAGG - 3′)* (Dharmacon, SMART®).

QUANTIFICATION AND STATISTICAL ANALYSIS

Single-cell RNA-seq data processing

Quality assessment of RNA-seq data was performed using FastQC (v0.11.4) (https://www.bioinformatics.babraham.ac.uk/projects/fastqc), FastQ Screen (v0.11.4) (https://www.bioinformatics.babraham.ac.uk/projects/fastq_screen), Kraken (v1.1) and visualized with MultiQC (v0.8). Reads were quality trimmed with Trim Galore! (v0.4.2, https://www.bioinformatics.babraham.ac.uk/projects/trim_galore/). Trimmed reads derived from xenograft models were aligned to human (GRCh38) and mouse (GRCm38) genomes using STAR (v2.5.2a) and assigned to either the human or mouse using disambiguate (v 1.0.0). Transcript-level expression of transcripts obtained from Ensembl release 89 was quantified using Salmon (v0.11.3, parameters–seqBias and–gcBias). Gene-level expression was obtained by aggregating transcript-level abundances using tximport. Quality control of processed data was performed with the scater package. Samples with at least 500'000 counts from endogenous genes, 8'000 features detected (threshold $\geq$ 1 count) and

showing less than 50% of counts from the 100 most expressed genes were retained for further analysis. Cell cycle was assigned to each sample using Seurat.

Differential expression

Differential expression (DE) between normoxic and hypoxic CTC clusters was computed with the likelihood ratio test method in the edgeR package (v3.20.1) and using the rounded length-scaled TPM as input. Genes detected in less than 25% of the samples (threshold 1 TPM) were removed prior to the DE analysis. To define hypoxia, we used a combined criterion defined by HypoxiaRed staining and hypoxia scoring based on gene expression. Hypoxia score was generated independently in each model (NSG-LM2, NSG-BR16 and BR61) by ranking samples according to their mean expression of *VEGFA* and *HIF1A* transcripts and calculating the fractional rank normalized between 0 and 1. Scores above the median were considered as positive. Hypoxic CTC clusters (n = 14) were defined as positive for both hypoxia score and HypoxiaRed. On the contrary, normoxic CTC clusters (n = 17) were defined as negative for both hypoxia score and HypoxiaRed. Samples with discordant results for both criteria were not considered for DE analysis.

Validation of the Hypoxic CTC cluster gene signature

The validation our hypoxia signature was performed using the dataset GSE109761 (Szczerba et al., 2019) from NCBI Gene Expression Omnibus (GEO). The dataset contains 62 single CTCs and 21 CTC clusters from a total of 13 breast cancer patients. Counts per million reads (CPM) were calculated after normalization using the size factors included in the SingleCellExperiment object. The expression matrix was standardized at gene-level (z-scores) using log2 (CPM+1) values as input. Hypoxia score was assigned to each sample by averaging the z-scores across the 25 genes upregulated in the signature. Bootstrapping approach was performed to account for higher dropout rate in single CTC compared CTC clusters. For this, an expression score was computed for 10'000 random sets of 25 genes in the same fashion as for hypoxia score, and the empirical distribution of the one-sided Student t-statistic comparing single CTC and CTC clusters was calculated. The bootstrapped *P value* obtained was 0.047.

Overall survival analysis using TCGA data

Harmonized gene expression quantification data of Breast Invasive Carcinoma Stage I samples of the Cancer Genome Atlas (TCGA-BRCA) was downloaded from the Genomic Data Commons Data Portal (GDC) using the TCGAbiolinks package. The expression matrix was constructed using the Fragments Per Kilobase of transcript per Million mapped reads normalized using upper quartile (FPKM-UQ) for each sample as obtained with the HTSeq workflow. Clinical data were obtained from the TCGA Pan-Cancer Clinical Data Resource (TCGA-CDR) and overall survival was defined as death from any cause. Hypoxia score (HS) on TCGA-BRCA data was constructed by calculating the mean of the gene-level standardized expression (z-scores) across the 25 genes found upregulated in hypoxic CTC clusters and the signatures developed by Buffa et al. (2010), Winter et al. (2007), Ragnum et al. (2015) and Elvidge et al. (2006). HS was then divided by quantiles and the overall survival of patients from Q1 and Q4 was compared using the Kaplan-Meier method using the survival package. The significance between both groups was assessed using the log-rank test. Time-dependent receiver operator curves (ROC) using a predictive time of 10 years were computed using the Nearest Neighbor Estimation (NNE) method implemented in the survivalROC package.

Distant metastasis-free survival

Distant metastasis-free survival analysis was performed on multiple microarray breast cancer studies from GEO using the online tool KM-plotter (https://kmplot.com/analysis/index.php?p=service&cancer=breast; accessed 31 October 2019). The mean expression across the optimal probes for the 25 genes found upregulated in hypoxic CTC clusters was used to divide samples into quartiles. A total of 664 patients were selected for the analysis with a maximum follow-up period of 10 years.

TMT-MS analysis

The acquired raw-files were converted to the mgf format and searched using the MASCOT algorithm (Matrix Science, Version 2.4.1). The mgf files were searched against database containing normal and reverse sequences of the of Uniprot entries *Homo sapiens* (2019/03/07), the six calibration mix proteins and commonly observed contaminants (in total 41,592 sequences for *Homo sapiens*). The MS1 ion tolerance was set to 10 ppm and fragment ion tolerance was set to 0.02 Da. The search criteria were set as follows: full tryptic specificity was required, 3 missed cleavages were allowed, carbamidomethylation (C), TMT6plex (K and peptide n-terminus) were set as fixed modification and oxidation (M) as a variable modification. Next, the database search results were imported to the Scaffold Q+ software (version 4.3.2, Proteome Software Inc., Portland, OR) and the protein FDR rate was set to 1%. Acquired reporter ion intensities in the experiments were employed for automated quantification and statics analysis using modified SafeQuant R script (v2.3). A q value < 0.1 was used as cutoff of significance. All the significant proteins were filtered for a unique entry name and run for gene ontology analysis using gProfiler web server and gProfileR package v 0.6.7.